

Antitumor Agents

Tunable Anticancer Activity of Furoylthiourea-Based Ru^{II}–Arene Complexes and Their Mechanism of Action

Srividya Swaminathan,^[a] Jebiti Haribabu,^[a] Naveen Kumar Kalagatur,^[b] Maroli Nikhil,^[c] Nithya Balakrishnan,^[a] Nattamai S. P. Bhuvanesh,^[d] Krishna Kadirvelu,^[b] Ponmalai Kolandaivel,^[e] and Ramasamy Karvembu*^[a]

Abstract: Fourteen new Ru^{II}–arene (*p*-cymene/benzene) complexes (**C1**–**C14**) have been synthesized by varying the *N*-terminal substituent in the furoylthiourea ligand and satisfactorily characterized by using analytical and spectroscopic techniques. Electrostatic potential maps predicted that the electronic effect of the substituents was mostly localized, with some influence seen on the labile chloride ligands. The structure–activity relationships of the Ru–*p*-cymene and Ru–benzene complexes showed opposite trends. All the complexes were found to be highly toxic towards IMR-32 cancer cells, with **C5** (Ru–*p*-cymene complex containing C₆H₂(CH₃)₃

as *N*-terminal substituent) and **C13** (Ru–benzene complex containing C₆H₄(CF₃) as *N*-terminal substituent) showing the highest activity among each set of complexes, and hence they were chosen for further study. These complexes showed different behavior in aqueous solutions, and were also found to catalytically oxidize glutathione. They also promoted cell death by apoptosis and cell cycle arrest. Furthermore, the complexes showed good binding ability with the receptors Pim-1 kinase and vascular endothelial growth factor receptor 2, commonly overexpressed in cancer cells.

Introduction

The growth of research in the field of medicinal chemistry has been highly beneficial for the well-being of humans. In a study that proved to be a boon to mankind, Barnett Rosenberg accidentally discovered the cytotoxic nature of cisplatin,^[1] a platinum-based compound that gained approval from the Food and Drug Administration (FDA) in 1978 and went on to become a widely used anticancer drug. After its discovery, the research on platinum-based anticancer drugs flourished, which led to the discovery of various new therapeutics, a couple of which were approved for the global market (Figure 1).^[1,2]

Although platinum-based drugs gained importance in cancer treatment, they came with serious drawbacks.^[3] In a search for alternatives, scientists began to explore options with other metal ions. Ruthenium complexes came foremost with desirable properties, which made them exciting candidates for medicinal applications. They were found to be selectively active toward cancer cells over normal cells, and to mimic iron in binding to biological molecules.^[4] The antineoplastic ruthenium frameworks that have entered clinical trials mostly involve Ru^{III} species, imidazolium (imidazole)(dimethyl sulfoxide)-tetrachlororuthenate(III) (NAMI-A), indazolium *trans*-tetrachlorobis(1*H*-indazole)ruthenate(III) (KP1019) and sodium *trans*-tetrachlorobis(1*H*-indazole)ruthenate(III) (KP1339; Figure 2).^[5] Numerous pharmaceutical chemists are exploring Ru^{II} scaffolds in preclinical studies that are at several stages of development. Namely, Ru^{II}–arene compounds containing ethylenediamine (en) or 1,3,5-triaza-7-phosphaadamantane (PTA) ligand have shown efficient antineoplastic activity. Another promising Ru^{II} therapeutic, TLD1433, has entered phase 1 and phase 2a clinical trials for non-muscle invasive bladder cancer treatment by photodynamic therapy (PDT).^[6]

[a] S. Swaminathan, Dr. J. Haribabu, N. Balakrishnan, Prof. R. Karvembu
Department of Chemistry, National Institute of Technology
Tiruchirappalli 620015, Tamil Nadu (India)
E-mail: kar@nitt.edu

[b] Dr. N. K. Kalagatur, Dr. K. Kadirvelu
DRDO-BU Centre for Life Sciences, Bharathiar University Campus
Coimbatore 641046, Tamil Nadu (India)

[c] Dr. M. Nikhil
Centre for Condensed Matter Theory, Department of Physics
Indian Institute of Science, Bangalore 560012, Karnataka (India)

[d] Dr. N. S. P. Bhuvanesh
Department of Chemistry, Texas A & M University
College station, Texas 77842 (USA)

[e] Prof. P. Kolandaivel
Periyar University, Salem 636011, Tamil Nadu (India)

Supporting information and the ORCID identification number(s) for the author(s) of this article can be found under:
<https://doi.org/10.1002/chem.202004954>.

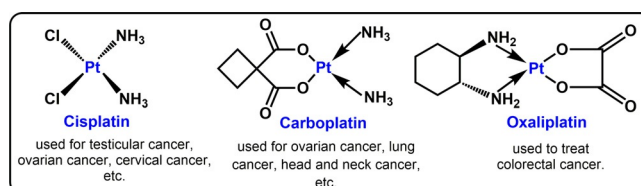


Figure 1. Globally approved platinum-based anticancer drugs.

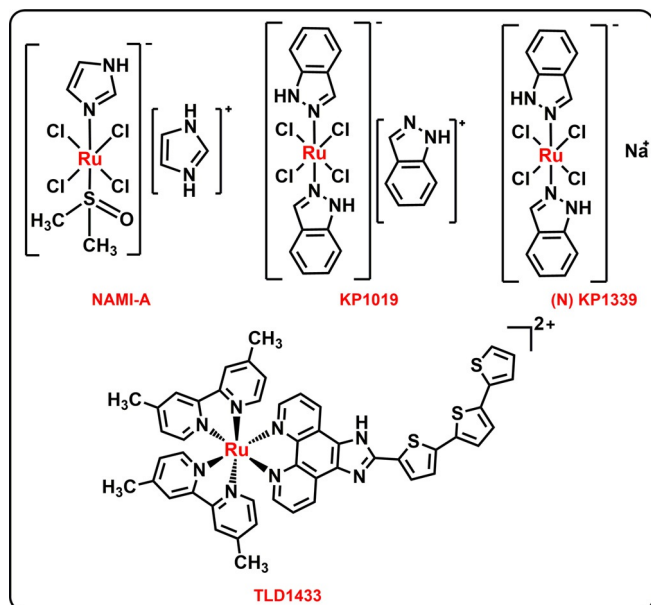
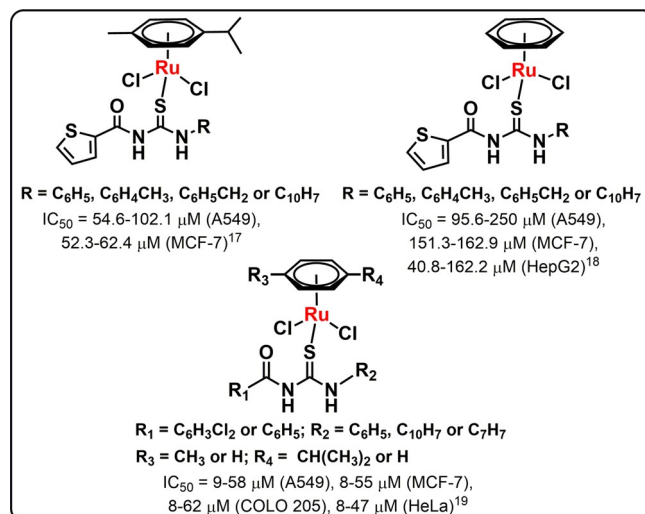


Figure 2. Ruthenium compounds in clinical trials.

Metals combined with organic motifs are becoming increasingly dominant with their vast number of applications.^[7–10] In the pharmaceutical industry, although many drugs in the market are seemingly organic in nature, organometallic compounds offer various benefits over their organic counterparts. They demonstrate a wide range of oxidation states, lipophilic character, redox properties, structural diversity, kinetic stability, an ability to bind to biomolecules and the opportunity to tune ligands to control the kinetic properties. In this regard, ligand selection needs to be carefully planned for the development of organometallic drugs.^[11–14] Aroylthioureas are known to exhibit antibacterial, antifungal, and anticancer properties. Our group has been actively investigating the biological properties of Ni^{II}, Pd^{II} and Cu^{II} complexes of aroylthiourea ligands.^[15,16] More recently, we have diverted our efforts towards aroylthiourea-based Ru^{II}–arene complexes, which have resulted in potential anticancer agents (Figure 3).^[17–19]

Although the literature contains a significant number of reports on Ru^{II}–arene acylthiourea complexes, the structure–activity relationships of these compounds have seldom been investigated. The structures of these compounds are similar to ruthenium–arene PTA (RAPTA) species, which make them interesting candidates for anticancer applications, because the latter are rapidly evolving as lead compounds for the treatment of cancer. Hence, in this study, we have explored the Ru^{II}–arene complexes of furoyl-based thiourea ligands for their anticancer properties, with the perspective that furan derivatives are important pharmaceutical compounds. Various substituents (electron-donating/electron-withdrawing/steric/different aliphatic chain length) on the terminal nitrogen were selected to study their effects.^[20,21] As a result, 14 Ru^{II}–*p*-cymene or Ru^{II}–benzene complexes with furoylthiourea ligands were synthesized. They were characterized and evaluated for their solution behavior, GSH binding and anticancer activity.

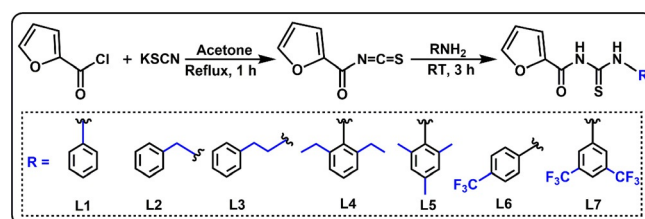
Figure 3. Aroylthiourea-based Ru^{II}–arene complexes reported by our group.

Results and Discussion

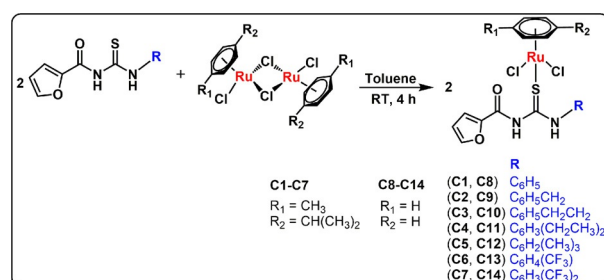
Synthesis

The ligands **L1**–**L7** were synthesized from 2-furoyl chloride, potassium thiocyanate and the respective amines according to a previously reported procedure (Scheme 1).^[16] Among these ligands, **L6** and **L7** are new, and they were characterized by elemental analysis and UV/Vis, FTIR and NMR spectroscopy.

The Ru^{II}–arene complexes were synthesized by adding the [Ru(arene)Cl₂]₂ (arene = *p*-cymene or benzene) precursor to a solution of the corresponding ligand in toluene (Scheme 2). A few drops of methanol were added to promote the solubility of the metal precursor.^[19] The reaction was allowed to proceed for 4 h, after which the ligand spot in TLC had completely disappeared. The resulting reaction mixture was concentrated



Scheme 1. Synthesis of the furoylthiourea ligands.

Scheme 2. Synthesis of the Ru^{II}–arene complexes.

under reduced pressure, and then hexane was added until a solid formed. The precipitate was filtered, washed thoroughly with hexane and dried under vacuum. The complexes were obtained in good yields (70–79%). Crystals of **C1–C4**, **C6**, **C8** and **C14** were grown in DMF/chloroform solution, and their structures were solved by single-crystal XRD analysis.

Spectroscopic characterization

The compounds were initially characterized by elemental analysis and UV/Vis and FTIR spectroscopy (see Figures S1–S16 and Tables S1 and S2 in the Supporting Information).^[17–19] The ^1H and ^{13}C NMR spectra of the ligands **L6** and **L7**, aside from their aromatic protons and carbon atoms being observed in their respective regions, showed amide and thioamide N–H protons as singlets in the ranges 12.53–12.50 and 11.62–11.45 ppm, respectively. The thioamidic and amidic carbon signals were seen at around 179.5–178.4 and 157.9–156.9 ppm, respectively. Each of the trifluoromethyl carbon atoms showed four signals in the ^{13}C NMR spectra in the range 126.3–119.9 ppm as a result of spin–spin coupling between the carbon and fluorine atoms (see Figures S17–S22).^[17,18]

In the ^1H NMR spectra of the complexes, the three aromatic protons of the furan ring were observed as two doublets and a doublet of doublets in the ranges 8.11–7.60 and 6.79–6.49 ppm, respectively. The terminal N substituents of the ligands, apart from the aromatic protons, which were observed in their respective regions, displayed signals as follows: the methylene protons were seen as a doublet at 4.86–4.79 ppm (**C2** and **C9**), the CH_2CH_2 protons as a doublet of doublets (3.94–3.92 ppm) and triplet (3.03 ppm; **C3** and **C10**), and the CH_2CH_3 protons as a multiplet and triplet at 2.62 and 1.22 ppm (**C4** and **C11**), respectively. The signals due to the *ortho*- and *para*-methyl protons of **C5** and **C12** appeared at 2.25 and 2.14 ppm as singlets, respectively. The aliphatic segments of the *p*-cymene ligand showed characteristic signals, that is, a doublet corresponding to the six protons of the isopropyl methyl groups at 1.35–1.19 ppm, a multiplet at 3.02–1.63 ppm due to the C–H proton and a singlet at 2.29–2.09 ppm caused by the methyl protons. Similarly, the aromatic protons of the *p*-cymene ring appeared as doublets in the ranges 5.83–5.32

and 5.79–5.21 ppm (**C1–C7**). The benzene complexes (**C8–C14**) each showed a sharp singlet corresponding to the six protons in the range 5.98–5.62 ppm.

The ^{13}C NMR spectra of the complexes showed a signal due to the thioamidic carbon (C=S) in the most shielded region (185.4–178.8 ppm), whereas the amidic carbon (C=O) signal was observed in the range 162.6–157.7 ppm. All the aromatic carbon atoms were observed in the expected region. The aliphatic carbon atoms of the *p*-cymene, that is, the methyl carbon attached to the aromatic ring, the isopropyl carbon and the two methyl carbons attached to the isopropyl carbon, displayed signals in the ranges 30.5–30.3, 22.3–21.9 and 18.4–18.2 ppm, respectively (**C1–C7**). In the spectra of the complexes with benzene as the arene moiety (**C8–C14**), an intense signal corresponding to the six carbon atoms was observed at around 92.8–85.3 ppm (see Figures S23–S54 in the Supporting Information). The ^{19}F NMR spectra of the compounds containing CF_3 were recorded and a single sharp peak was observed for all in the range 60.5–61.5 ppm (see Figures S19, S22, S35, S38, S51 and S54).

The mass spectra of the complexes showed a base peak corresponding to the $[\text{M}-2\text{H}^+-2\text{Cl}^-+\text{H}^+]^+$ fragment, in agreement with the data reported for similar types of complexes in the literature (see Figures S55–S68 in the Supporting Information).^[17–19]

Molecular structures

The structures of **C1–C4** and **C6** (Ru-*p*-cymene complexes), and **C8** and **C14** (Ru-benzene complexes) were determined by single-crystal XRD analysis. The complexes showed a pseudo-octahedral geometry around the ruthenium ion with a piano stool form (Figure 4 and Tables S3 and S4 in the Supporting Information).^[22–24] On going from **C1** (2.405 Å) to **C3** (2.4206 Å), there was a noticeable increase in the Ru–S bond length, owing to the distancing of the phenyl group from the thiocarbonyl (C=S) moiety. This increase was also observed in the case of **C4** (2.4065 Å), in which electron-donating ethyl groups are attached at the *ortho* positions of the terminal phenyl moiety, from which it can be concluded that the Ru–S bond becomes weaker in such cases. In contrast, the Ru–S bond was

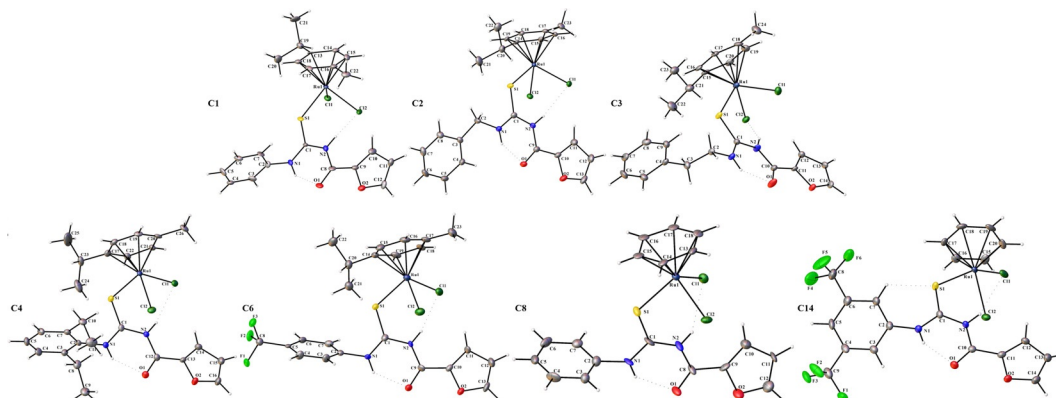


Figure 4. Crystal structures of the complexes **C1–C4**, **C6**, **C8** and **C14**.

shorter in **C6** (2.4025 Å), and still shorter in **C14** (2.3875 Å) compared with their parent complexes **C1** and **C8** (2.406 Å), respectively, which signifies the strengthening of the bond in the presence of electron-withdrawing group(s). The Ru–C bond lengths in the arene rings showed similar trends.

It is interesting to note that the Ru–S bond in benzene complex **C8** was longer than that in its *p*-cymene analogue **C1**. This may be because the electron-donating groups on *p*-cymene reduce its π -accepting ability, which result in longer Ru–arene and shorter Ru–S bonds (Table 1).

In addition, an increase in the Cl–Ru–Cl angle was observed upon moving from **C1** (87.54°) to **C3** (87.96°), which might be attributed to the fact that the bulky phenyl group is further away from the metal center, thereby allowing the chloride ligands to assemble freely in space. Further proof for this was observed in a contrasting manner when the same angle was lower in **C4** (86.95°) due to the steric effect of the ethyl groups present in both of the *ortho* positions of the phenyl substituent. Comparing the Cl–Ru–Cl angles of **C1** (87.54°) and **C6** (91.96°), and **C8** (86.85°) and **C14** (87.79°), the angle showed a noticeable increase with the electron-withdrawing group(s) attached to the terminal N of **C6** and **C14**, which may be due to the shortening of the Ru–S bond in these complexes placing the sulfur atom and chloride ligands in a crowded environment. The N–H bond distances (0.88 Å) in all the complexes were almost the same. All the bond lengths and angles of these complexes are in good agreement with those of similar compounds reported in the literature.^[17–19]

Table 1. Selected bond lengths in **C1–C4**, **C6**, **C8** and **C14**.

	Bond lengths [Å]						
	C1	C2	C3	C4	C6	C8	C14
Ru1–Cl1	2.416	2.418	2.410	2.412	2.403	2.420	2.414
Ru1–Cl2	2.431	2.434	2.426	2.439	2.426	2.425	2.408
Ru1–S1	2.405	2.416	2.420	2.406	2.402	2.406	2.387
Ru1–C13	2.206	2.189	2.189	2.205	2.189	2.230	2.189
Ru1–C14	2.203	2.169	2.172	2.177	2.165	2.170	2.183
Ru1–C15	2.195	2.207	2.187	2.183	2.172	2.173	2.164
Ru1–C16	2.200	2.169	2.223	2.219	2.212	2.197	2.176
Ru1–C17	2.185	2.189	2.199	2.188	2.179	2.160	2.173
Ru1–C18	2.175	2.197	2.162	2.166	2.193	2.183	2.206
N1–H1	0.880	0.880	0.880	0.880	0.880	0.880	0.880
N2–H2	0.880	0.880	0.880	0.880	0.880	0.880	0.880
S1–C1	1.704	1.709	1.709	1.700	1.689	1.713	1.683
O1–C8	1.220	1.225	1.223	1.232	1.218	1.226	1.228

Theoretical studies using DFT

The results of density functional theory (DFT) calculations verified the structures obtained from single-crystal XRD analysis as well as the diamagnetic character of Ru^{II} in the studied complexes (see Figures S69–S71 and Tables S5 and S6 in the Supporting Information).^[25–30] The electrostatic potential (ESP) surface diagrams (see Figure S70) revealed that the electron density is highest on the two chloride ligands, the carbonyl oxygen and the oxygen of furan.^[27,28] The effect of the electron-donating/withdrawing substituents on the furylthiourea

ligand is mostly observed as a localized effect.^[21] The ESP of the ligand exposed enhanced/diminished electronic charge density on the terminal N to which the substituent was attached. There was no significant effect observed for complexes **C1–C3** and **C8–C10**. The electron-donating groups in complexes **C4**, **C5**, **C11** and **C12** generated a more negative ESP within the terminal *N*-substituted aromatic ring, whereas the complexes with electron-withdrawing substituents (**C6**, **C7**, **C13** and **C14**) provided a more positive ESP within the ring. The calculations also showed that the chloride ligands of **C6**, **C7**, **C13** and **C14** (containing electron-withdrawing substituents) displayed a less negative ESP than those of **C4**, **C5**, **C11** and **C12** (containing an electron-donating substituent).

Anticancer potential

The *in vitro* anticancer activities of the complexes were evaluated by an MTT (3-(4,5-dimethylthiazol-2-yl)-2,5-diphenyltetrazolium bromide) assay in five different cancer cell lines (A431-epidermoid carcinoma, HeLa-cervix, HepG2-liver, IMR-32-neuroblastoma and SW40-colorectal cancer; Figure 5) and one normal cell line (Vero; see Figure S72 in the Supporting Information).^[31,32]

The IC₅₀ values of the complexes are compiled in Table 2. The complexes showed highest activity in the human neuroblastoma cell line (IMR-32) with the lowest IC₅₀ values determined for complexes **C5** (11.34 ± 0.42 μM) and **C13** (11.84 ± 0.66 μM). Although the anticancer potential of the complexes was lower than that of the positive control cisplatin, it was comparable to or even greater than those of other reported complexes after an incubation period of just 24 h.^[33–36] We could see that the IC₅₀ values of the complexes mostly decreased as the *N*-substituted phenyl moved away from the furylthiourea group. Interestingly, for the *p*-cymene complexes (**C1–C7**), electron-donating substituent(s) in the phenyl ring attached to the terminal N lowered the IC₅₀ values of the complexes. In contrast, the electron-withdrawing groups exerted the same influence in the benzene analogues (**C8–C14**). The IC₅₀ values of the complexes in the normal cell line (Vero) were almost three-fold greater than those observed in the cancer cell lines, which reveals the selectivity of the complexes. Owing to their highest activities and contrasting behavior, **C5** and **C13** were chosen from each set and subjected to further mechanistic studies.

Since the discovery of metal-based anticancer drugs, it has been of the utmost importance to find the mechanism of operation of these compounds inside the human body.^[37–39] Thus, the mechanistic pathway by which the most active complexes **C5** and **C13** cause cell death has been investigated, as detailed in the following.

Solution behavior of **C5** and **C13**

The solution behavior of **C5** and **C13** was studied by using UV/Vis spectrophotometry under a variety of conditions. The UV/Vis spectra of **C5** and **C13** at 298 K immediately after dissolution in water (water/DMSO, 9.9:0.1, v/v; see Figure S74 in the

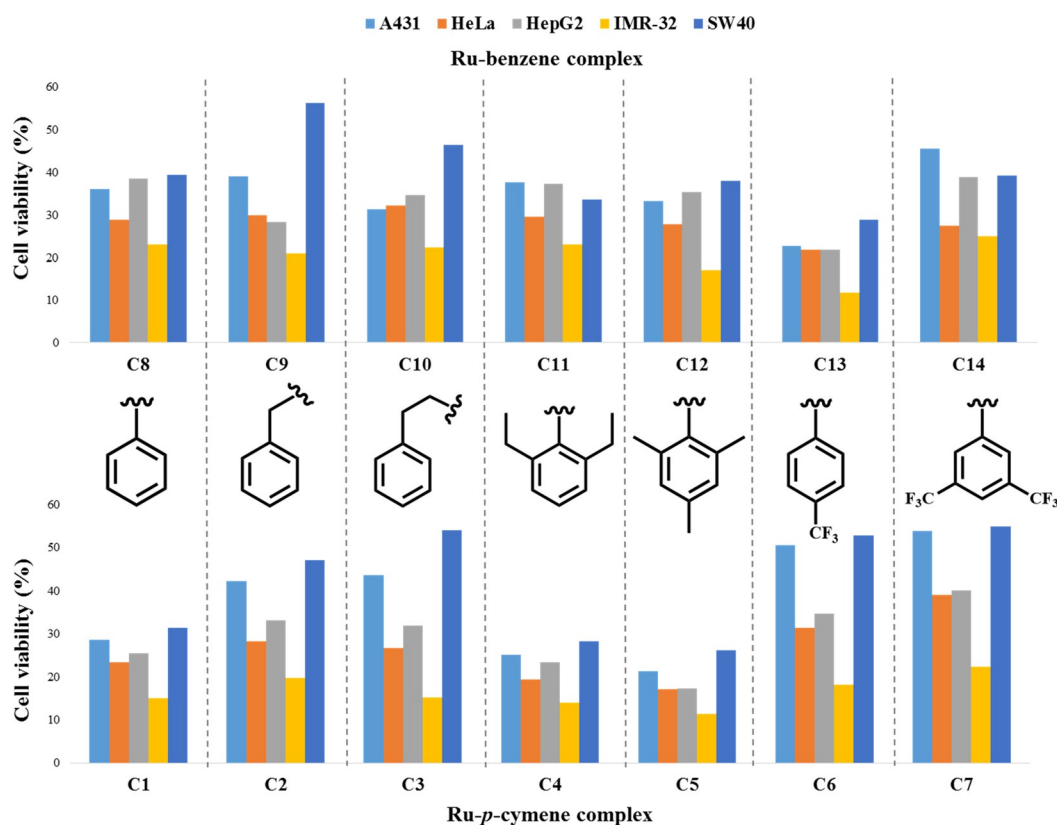


Figure 5. Variation in the cell viability [%] of the complexes with change in the *N*-terminal substituent.

Complex	IC ₅₀ [μM]					
	A431	HeLa	HepG2	IMR-32	SW40	Vero
C1	28.5 ± 1.2	23.3 ± 0.8	25.5 ± 0.1	15.0 ± 1.0	31.4 ± 0.1	107.2 ± 2.3
C2	42.2 ± 0.6	28.2 ± 1.2	33.1 ± 0.6	19.6 ± 0.6	47.1 ± 0.4	121.1 ± 2.0
C3	43.5 ± 0.4	26.6 ± 1.3	31.9 ± 0.3	15.1 ± 0.9	54.0 ± 1.5	119.6 ± 3.8
C4	25.1 ± 0.5	19.2 ± 0.6	23.3 ± 0.5	13.9 ± 0.9	28.2 ± 0.7	95.9 ± 4.0
C5	21.3 ± 1.0	17.0 ± 1.0	17.2 ± 0.6	11.3 ± 0.4	26.2 ± 0.1	91.8 ± 4.6
C6	50.5 ± 0.4	31.3 ± 0.4	34.7 ± 1.2	18.1 ± 0.8	52.8 ± 1.7	121.9 ± 3.9
C7	53.8 ± 1.6	39.0 ± 0.9	40.1 ± 0.2	22.3 ± 0.1	54.9 ± 1.3	126.3 ± 1.7
C8	36.1 ± 0.3	28.8 ± 1.2	38.4 ± 0.9	23.0 ± 0.5	39.5 ± 0.6	130.0 ± 3.7
C9	39.1 ± 1.1	29.9 ± 0.7	28.3 ± 1.3	20.9 ± 0.6	56.2 ± 1.8	112.0 ± 2.0
C10	31.3 ± 0.7	32.2 ± 0.1	34.6 ± 1.5	22.2 ± 0.9	46.4 ± 1.0	133.3 ± 0.4
C11	37.7 ± 1.7	29.5 ± 0.6	37.3 ± 0.4	23.0 ± 0.5	33.6 ± 0.7	117.1 ± 2.1
C12	33.2 ± 1.3	27.8 ± 0.6	35.3 ± 0.5	17.0 ± 0.6	38.0 ± 1.3	134.5 ± 1.3
C13	22.6 ± 0.7	21.8 ± 0.7	21.7 ± 0.6	11.8 ± 0.7	28.8 ± 0.4	93.8 ± 4.1
C14	45.5 ± 1.0	27.4 ± 0.2	38.9 ± 1.1	24.9 ± 1.1	39.2 ± 1.3	116.7 ± 2.6
cisplatin	9.8 ± 0.8	6.1 ± 0.5	7.9 ± 0.2	5.7 ± 0.6	7.12 ± 0.3	16.7 ± 1.3

Supporting Information) exhibited a strong absorption band at around 280 nm that underwent a small hypsochromic shift while decreasing in intensity over time, concomitant with the appearance of a new shoulder peak at around 330 nm, the intensity of which increased with time, indicating rapid hydrolysis of the complexes, although the exact nature of the hydrolysis products was not known until later.^[40–42] The hydrolysis process seemed to attain equilibrium after 25 min for both complexes.

To investigate the suppression of hydrolysis by chloride ions, the UV/Vis spectra of C5 and C13 (0.5 mM) were recorded at 298 K in 4 mM NaCl solution. The spectra were essentially the same as those observed in water, which indicates that a low chloride concentration did not suppress hydrolysis. However, the spectra of the complexes dissolved in a higher concentration of NaCl (100 mM) revealed that the hydrolysis was suppressed (Figure 6). These results indicate that these complexes, unless metabolized in a different way, for example, by protein

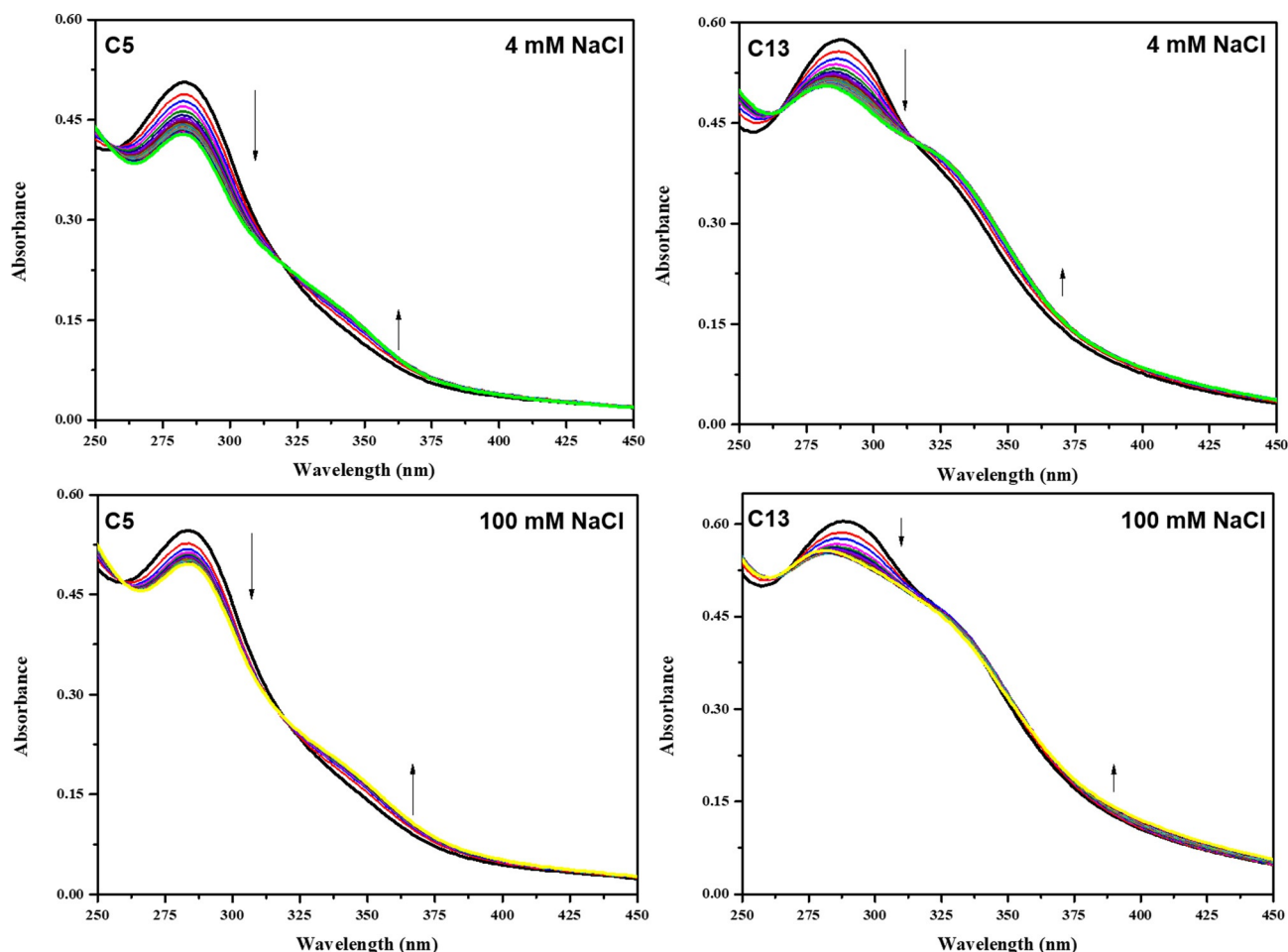


Figure 6. Time-dependent UV/Vis absorption spectra of C5 and C13 in 4 and 100 mM NaCl at 298 K, recorded at 1 min intervals over a period of 30 min.

binding, may be able to survive the conditions found in the bloodstream, and that hydrolysis may take place inside the cells in which the chloride concentration decreases to around 4 mM.^[41]

The time-dependent absorption spectra (difference spectra) of C5 and C13 in 100 mM aqueous NaClO₄ at 298 K are shown in Figures S75 and S76 in the Supporting Information. In each case, the presence of two isosbestic points (C5: 274 and 326 nm; C13: 281 and 324 nm) suggested the hydrolysis of the chloro complexes. The maximum change in absorption occurred at 285 and 295 nm for C5 and C13, respectively, and hence these wavelengths were selected for subsequent kinetic studies.^[42] The hydrolysis of C5 and C13 at 298 K in aqueous NaClO₄ (0.015–0.5 M) was monitored at the selected wavelengths (see Figure S77). In each case, the time-dependent absorbance followed first-order kinetics; the corresponding rate constants (k_{obs}) are listed in Table 3. For both complexes, the rate of hydrolysis was almost independent of ionic strength. The reverse reaction was too rapid to be studied by UV/Vis spectrophotometry.

The aqueous solution chemistry of C5 and C13 was studied in detail at 298 K over 24 h by ¹H NMR spectroscopy and ESI-MS spectrometry. Due to the low solubility of the complexes in water, the NMR studies were conducted in 3:7 (v/v) [D₆]DMSO/

Table 3. Rate constants and half-lives for the hydrolysis of complexes C5 and C13 in various strengths of NaClO₄.

	[NaClO ₄] [M]	0.015	0.1	0.25	0.5
C5	k_{obs} [10^{-3}s^{-1}]	1.38 ± 0.001	1.41 ± 0.005	1.35 ± 0.002	1.39 ± 0.002
	$t_{1/2,\text{obs}}$ [min]	8.4	8.2	8.5	8.3
C13	k_{obs} [10^{-3}s^{-1}]	1.67 ± 0.005	1.79 ± 0.005	1.63 ± 0.006	1.64 ± 0.004
	$t_{1/2,\text{obs}}$ [min]	6.9	6.5	7.1	7.0

D₂O. The exchangeable protons present in the complexes disappeared immediately after the addition of D₂O. Further analysis of the ¹H NMR spectra revealed rapid hydrolysis of the complexes, leading to a mixture of compounds with arene loss (that is, products in which the three coordination sites originally occupied by the arene and chloride ligands were occupied by solvent molecules). Separate sets of peaks were observed for the chloride, aqua and arene-loss species (Figure 7). The loss of the arene was inferred by the presence of resonances for free *p*-cymene ($\delta \approx 7.23$ ppm (dd)) and benzene ($\delta \approx 7.32$ ppm (s)) in the aromatic region for C5 and C13, respectively. Almost 85% of the complexes were hydrolyzed within 30 min, and the major hydrolyzed product constituted 75% of the products. The equilibria appeared to be reached quickly,

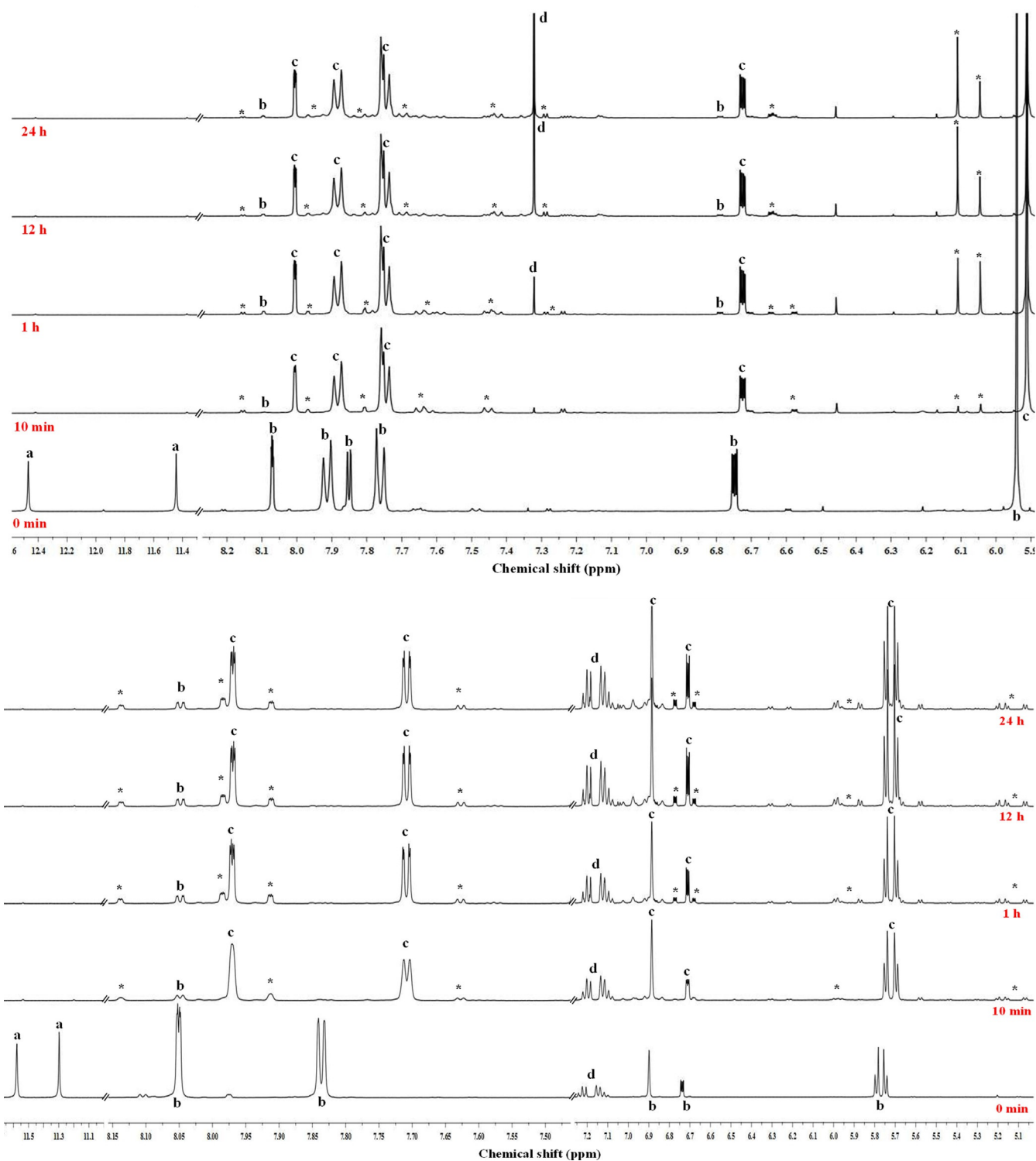


Figure 7. ^1H NMR spectra of **C5** (bottom) and **C13** (top) in 3:7 $[\text{D}_6]\text{DMSO}/\text{D}_2\text{O}$ at 298 K recorded over a period of 24 h. Peak assignments: a, exchangeable protons of intact chloride complex; b, intact chloride complex; c, predominant hydrolyzed species; d, free arene; *, other aquated/hydrolyzed species.

because the spectra recorded after 12 and 24 h showed insignificant changes in comparison with those recorded after 1 h. After 24 h, the original complex species accounted for less than 10% of species, and arene loss of around 7 and 27% was observed for **C5** and **C13**, respectively (based on peak integrals).^[43–46]

ESI-MS analysis of the complexes in 3:7 (v/v) $\text{DMSO}/\text{H}_2\text{O}$ after 24 h revealed the mononuclear $[\text{Ru}(\eta^6\text{-}p\text{-cymene})(\text{L5})(\text{Cl})(\text{H}_2\text{O})]^+$ to be the major hydrolysis species deriving from **C5**. However, the hydrolysis product of **C13** was observed to be a dimer, $\{[\text{Ru}(\eta^6\text{-benzene})_2(\text{L6})(\text{OH})_2(\text{H}_2\text{O})]^{2+}\}_2$, formed along with other minor products (see Figures S78 and S79 in the Support-

ing Information). This might be because benzene as an arene ligand is known to exhibit a strong *trans* labilizing effect on aqua ligands.^[44] The rate of hydrolysis of **C13** was higher than that of **C5**, although the more electron-accepting arene ligand in the former should lower the hydrolysis rate. However, the electron-withdrawing CF₃ substituent in **C13** weakens the donor ability of the ligand, thereby leading to an increase in the hydrolysis rate. In summary, the hydrolysis rates are tunable within this family of ruthenium–arene complexes, which is potentially useful in the design of anticancer drugs.^[37]

Binding with GSH

The tripeptide glutathione (γ -L-Glu-L-Cys-Gly; GSH) is an abundant (mM) intracellular thiol that is known to cause the detoxification of heavier transition-metal ions, including several platinum and ruthenium anticancer compounds, which have an affinity towards sulfur.^[47] However, Wang et al. reported a possibly conflicting role of GSH in the mechanism of action of Ru^{II}–arene complexes, which may contribute to the lack of cross-resistance for platinum-based therapeutics.^[48,49] The interaction of complexes **C5** and **C13** with GSH was studied by ¹H NMR spectroscopy; the spectra were recorded over a period of 24 h, after the addition of a known amount of the respective complex in [D₆]DMSO to a 10-fold excess concentration of GSH in D₂O (see Figure S80 in the Supporting Information). The experimental conditions were the same as used in the solution stability studies. The complexes immediately bound to GSH, as indicated by the observed spectral changes in comparison with the spectrum of free GSH. This could have an important impact on the biological activity of the Ru^{II}–arene complexes.^[50] After 12 h, new peaks attributable to the oxidized product GSSG arose in the spectra of the complexes.^[51] However, the intensity of these signals was lower in the spectrum of **C5** than in the spectrum of **C13**. This is perhaps not surprising because the electron-donating groups attached to furoylthiourea decreases its ability to oxidize GSH.^[52] On the basis of these studies, it is plausible that these complexes act as catalysts for the oxidation of GSH to GSSG. This also could explain why the Ru–*p*-cymene and Ru–benzene complexes show reverse activity on varying the substituents. As benzene is already a good π -acceptor ligand, the addition of electron-withdrawing group(s) to the ligand makes the metal ion less electron-dense, which makes it more susceptible to bind to GSH, and may reduce the level of GSH/GSSG in the cell, and hence promote apoptosis. However, the methyl and isopropyl groups in *p*-cymene tend to decrease its π -acidic properties, so the electron-withdrawing substituent in the ligand does not have much influence. Nevertheless, the presence of electron-donating groups in the ligand may increase the π -electron cloud of the planar rings, and subsequently the intercalation and distortion of DNA, leading to apoptosis.

Cell death pathway

Complexes **C5** and **C13** were subjected to bright-field microscopy, intracellular reactive oxygen species (ROS), mitochondrial

membrane potential (MMP), DNA damage and caspase-3 analyses to further elucidate their mechanism of action on IMR-32 cancer cells.

Bright-field microscopy was preliminarily employed to explore the micromorphology of the cells in the presence and absence of the complexes. Cisplatin was employed as a positive control. The control cells were seen to be healthy, with cell bodies and dendrites characteristic of neuronal cells. On treating the IMR-32 cells with IC₅₀ and IC₉₀ concentrations of the complexes, changes such as the leakage of cellular debris, damage to the cellular membrane and the formation of apoptotic bodies were visualized (Figure 8).^[19]

Cancer cells, which are metabolically altered, have higher ROS levels than normal cells. Therefore, they tend to reach the ROS threshold faster and are at a greater risk of undergoing apoptosis. Hence, a complex that can further promote ROS production in a cancer cell is probably an excellent drug candidate to induce cancer cell death. Keeping this in mind, the ROS levels in IMR-32 cells in the presence and absence of the complexes were measured by using the dichlorodihydrofluorescein diacetate (DCFH-DA) staining assay (Figure 9).^[53–55] Cisplatin was used as a positive control. An increase in fluorescence intensity was observed when the cancer cells were treated with IC₅₀ and IC₉₀ concentrations of the complexes as compared with the control cells. The fluorescence intensity was higher with the IC₉₀ concentration for both complexes. Notably, the complexes showed dose-dependent generation of ROS (see Figure S81 in the Supporting Information).

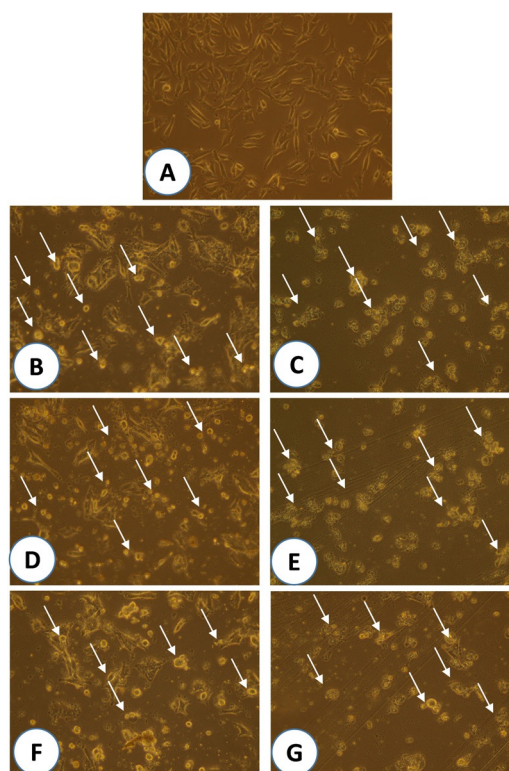


Figure 8. Bright-field microscopic images. (A) IMR-32 control cells. Cells treated with IC₅₀ and IC₉₀ concentrations of (B,C) cisplatin, (D,E) **C5** and (F,G) **C13**, respectively. The arrows indicate the leakage of cellular debris, damage to the cellular membrane and the formation of apoptotic bodies.

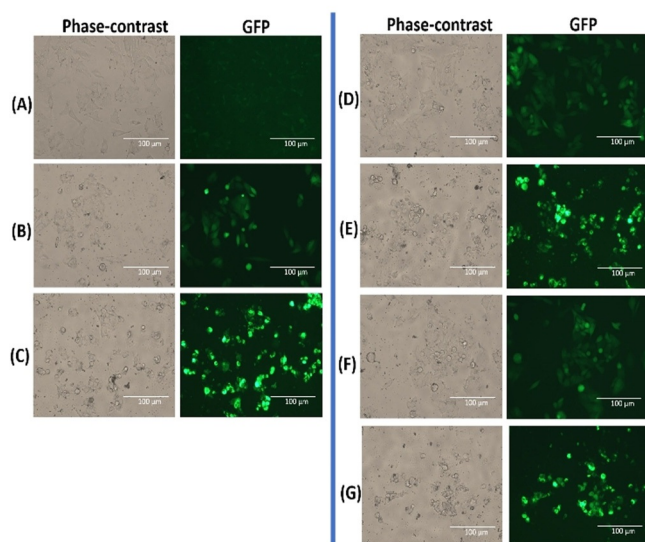


Figure 9. DCFH-DA-stained images. (A) IMR-32 control cells. Cells treated with IC_{50} and IC_{90} concentrations of (B,C) cisplatin, (D,E) **C5** and (F,G) **C13**, respectively. *GFP = green fluorescent product.

Having proved that the complexes generate ROS species in vitro, we next carried out the MMP analysis. A crucial step in intrinsic apoptosis is the increase in the permeability of the mitochondria, which results in a dramatic loss of its electrical potential, following which cytochrome c may be released.^[19,56] Rhodamine 123 (3,6-diamino-9-[2-(methoxycarbonyl)phenyl]-xanthylium chloride) is a cationic dye used to measure MMP. The green fluorescence of rhodamine 123 should decrease after the addition of a complex, which means that the electrical potential of the mitochondria has reduced. This was observed when the cancer cells were treated with both the complexes and the stain (Figure 10). Again, a dose-dependent de-

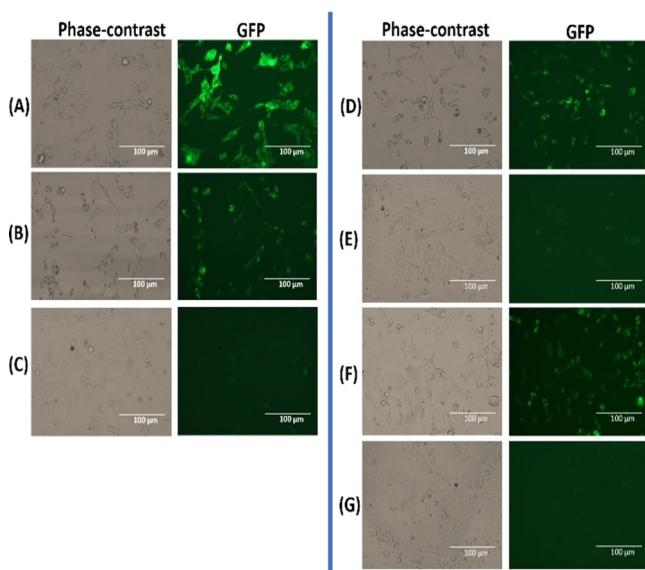


Figure 10. Rhodamine 123-stained images. (A) IMR-32 control cells. Cells treated with IC_{50} and IC_{90} concentrations of (B,C) cisplatin, (D,E) **C5** and (F,G) **C13**, respectively.

crease in the fluorescence intensity was observed. Also, the fluorescence was lower with the IC_{90} concentration of the complexes (see Figure S81 in the Supporting Information).

After the loss of MMP, which may lead to the release of cytochrome c, the next step in the intrinsic apoptosis pathway would be a cascade of caspases. Cytochrome c is known to activate caspase-9 by promoting nucleotide binding to apoptotic protein activating factor-1 (APAF-1), which in turn leads to the activation of caspase-3. Hence, caspase-3 analysis was carried out to prove the overexpression of caspases, which would confirm the apoptotic process. We observed a dose-dependent increase in caspase-3 for **C5** and **C13**, which indicates that the apoptotic process might have occurred in the IMR-32 cancer cell line.^[57] 4',6-Diamidino-2-phenylindole (DAPI) is a well-known bright-blue fluorescent, the intensity of which increases 20-fold on binding to double-stranded DNA preferentially at adenine-thymine (A-T) abundant zones. The fluorescence intensity exhibited by the cells treated with IC_{50} and IC_{90} concentrations of the complexes was higher than that exhibited by the control cells, which evidences conclusively that the complexes induced DNA damage and nuclear leakage in the IMR-32 cancer cells (Figure 11 and Figure S81 in the Supporting Information).^[58,59]

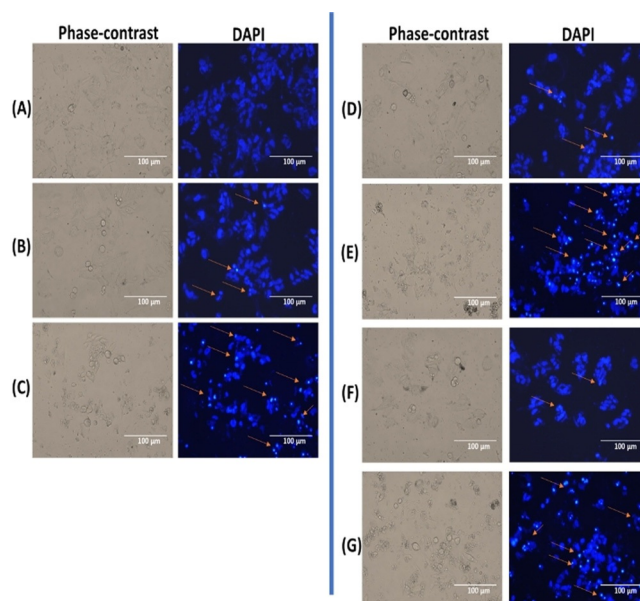


Figure 11. DAPI-stained images. (A) IMR-32 control cells. Cells treated with IC_{50} and IC_{90} concentrations of (B,C) cisplatin, (D,E) **C5** and (F,G) **C13**, respectively.

Cell cycle arrest

A cell that undergoes division renews itself in four phases, denoted G0-G1, S, G2 and M. The amount of DNA in a cell over varying periods can be determined by cell cycle analysis. The IMR-32 cell line was subjected to such analysis for 24 h following the addition of complexes **C5** and **C13** at their IC_{50} concentration, with cisplatin being used as a positive control.^[59]

The cell cycle diagrams depict the progression of the cell from G0-G1 to the G2-M phase (Figure 12). The percentages of

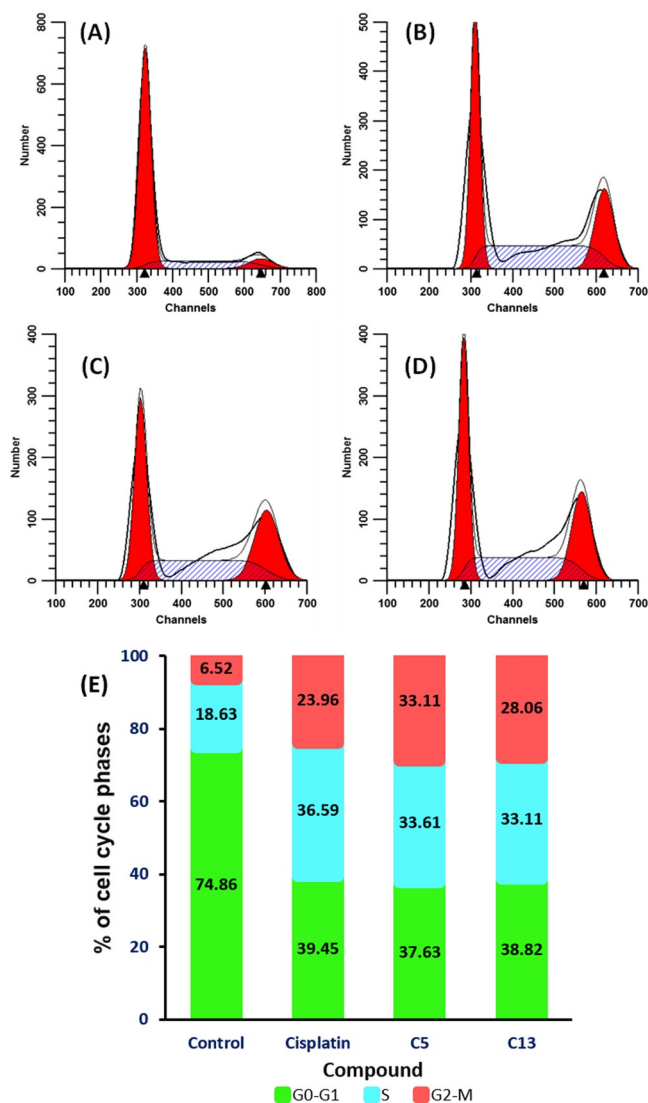


Figure 12. Cell cycle analysis of (A) control cells and cells treated with the IC_{50} concentration of (B) cisplatin, (C) **C5** and (D) **C13**. (E) Comparison of the percentages of cell cycle phases of cells treated with the complexes.

the G0-G1, S and G2-M phases in the control were found to be 74.86, 18.63 and 6.52%, respectively. When the cells were treated with the IC_{50} concentration of the complexes, the percentages decreased for G0-G1 and increased for the S and G2-M phases with respect to the control. It was observed that the complexes showed comparable activity to that of cisplatin. Notably, the changes in the percentages of cells in the S and G2-M phases on going from the control to the complexes were almost two- and four-fold, respectively, which indicates that the complexes mainly arrest the cell cycle in the latter phases of the process.

Apoptotic mode of cell death

Cellular apoptosis of **C5** and **C13** was studied at their IC_{50} concentration, with cisplatin as a positive control. As depicted in Figure 13, clockwise from top left, dead cells, late apoptosis,

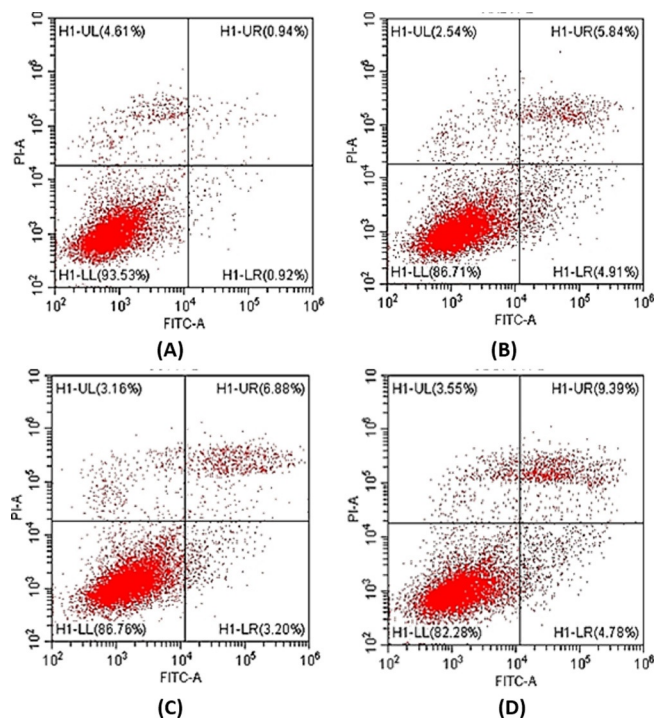


Figure 13. Flow cytometric analysis of (A) control cells and cells treated with the IC_{50} concentration of (B) cisplatin, (C) **C5** and (D) **C13**.

early apoptosis and viable cells are limited to each quadrant. It can be seen that cisplatin achieved an apoptosis rate of 10.75% (4.91% of early apoptosis and 5.84% of late apoptosis), whereas **C5** and **C13** achieved 10.08% (3.20% of early apoptosis and 6.88% of late apoptosis) and 14.17% of apoptosis (4.78% of early apoptosis and 9.39% of late apoptosis), respectively. Although both complexes gave comparable percentages of early and late apoptotic cells to those of cisplatin, **C13** exhibited better activity than the other two. These results confirm that the complexes prompted cancer cell death through an apoptotic pathway.^[59]

Interaction with protein receptors

Meggers and co-workers described how the unique shapes of metal complexes can be exploited for targeting enzymes and proteins. The Ru^{II} -arene complexes are known to exert a "multi-targeted" approach, that is, not only do they target DNA, but they also contain vectors to enable them to target cancer cells selectively and/or moieties that target enzymes, peptides and intracellular proteins.^[60,61] The Pim-1 kinase receptor has direct involvement in the regulation of cell cycle progression and apoptosis, and is overexpressed in various cancers such as prostate cancer, Burkitt's lymphoma and oral cancer, in addition to several hematopoietic lymphomas, whereas its deficiency leads to failure in cell survival and growth.^[62] The principal responder to the vascular endothelial growth factor signal, which regulates endothelial migration and proliferation, is vascular endothelial growth factor receptor 2 (VEGFR2).^[63] The VEGFR2 receptor has been reported to be

expressed in carcinomas and lymphomas, in addition to its expression in endothelial cells and vascular tumors, which makes it a crucial cell type marker. Hence, these two receptors were chosen for this study to explore the possible interactions between complexes **C5** and **C13** and the receptors. The optimized geometries of complexes **C5** and **C13** were used to perform molecular docking experiments with the Pim-1 kinase and VEGFR2 receptors (Figure 14).

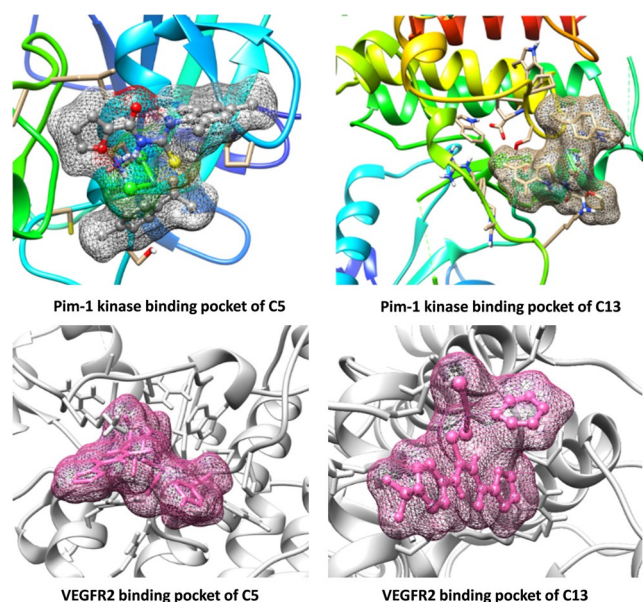


Figure 14. Molecular docking images for **C5** and **C13**.

The complexes formed hydrogen-bonding interactions with the surrounding amino acid residues of Pim-1 kinase, as well as strong electrostatic attractions, namely π -alkyl, π - π and π -sulfur interactions, at the binding site. The presence of the metal ion and high-affinity atoms such as chlorine contributed to the higher interaction energies of **C5**. Hydrogen-bonding interactions were also observed with residues of VEGFR2, along with strong alkyl and π -alkyl interactions at the active binding

sites of the receptor. All the interactions of the complexes with the individual proteins are listed in Table 4. The high binding energy and presence of electrostatic energy clouds in the binding sites will lead to structural changes in the receptors, which inhibit the functions of the proteins.

Conclusions

Fourteen new Ru^{II}-*p*-cymene/benzene complexes **C1**–**C14** have been synthesized and characterized by UV/Vis, FTIR and NMR spectroscopy as well as by mass spectrometry. The pseudo-octahedral geometries of the Ru^{II}-arene complexes were confirmed by a single-crystal XRD study, which revealed that the Ru–S bond weakened as the phenyl ring moved away from the furoylthiourea core or when there was an electron-donating group on the terminal N. On the other hand, an electron-withdrawing group on the terminal N strengthened the coordination bond. Theoretical calculations revealed that changes in the N substituent of the furoylthiourea ligand have a localized effect on the complex system, with minor changes in the ESPs of the chloride ligands.

All the complexes were screened for their anticancer potential by means of the MTT assay in five different cancer cell lines and were found to be highly toxic towards the IMR-32 cell line, while showing lower toxicity towards a normal cell line. To study their mechanism of action, complexes **C5** and **C13** were subjected to stability studies, and a preliminary investigation showed that the complexes underwent rapid hydrolysis. The reaction followed pseudo-first order kinetics, and the rate for **C13** was found to be higher than that for **C5**. The dominant species obtained from the hydrolysis of the former turned out to be a dinuclear complex, whereas the latter gave a mononuclear complex. Complex **C13** also proved to be a better catalyst for the oxidation of GSH to GSSG. A series of staining assays revealed the presence of ROS species, a reduction in the MMP and nuclear damage. Furthermore, the complexes could arrest the cell cycle. Flow cytometry studies confirmed the mechanism of cell death to be apoptotic. Interestingly, the complexes were capable of binding to receptors such as Pim kinase-1 and VEGFR2, which may help to block their functions.

Table 4. Interactions of **C5** and **C13** with the receptors Pim-1 kinase and VEGFR2.

	Protein receptor	Hydrogen-bonding interactions	Electrostatic interactions	Binding Energy [kcal mol ⁻¹]
C5	Pim-1 kinase	Pro87, Met88, Val91, Leu192, Val90, Trp198, His157, Val91, Cys158, Cys161	Leu192, Met88, Leu92, Pro81, Lys94, Val90, Cys161	–10.2
	VEGFR2	Thr24, Ser23, Arg927, Ser1098, Gly1100, Pro1066, Pro1103, Leu1099, Arg930, Arg27	Lys1060, Ala1101, Pro1066, Leu1027, Pro1105	–9.83
C13	Pim-1 kinase	Ser261, Glu262, Cys263, Leu266, Trp269, Ala272, Glu283, Thr280, His287, Ile284	Leu152, Trp146, Phe148, Arg145, Met290, His25, Leu266, His265, Trp149	–8.91
	VEGFR2	Cys1022, Leu910, Ser882, Met881, Arg1020, Leu1017, Phe1016, Leu828, Pro819, His877, Ile890	Cys1022, Arg1020, Leu1017, Phe1016, Leu828, Pro819, His877	–9.66

The study concluded that the anticancer activity of a bifunctional Ru^{II}-arene fuoylthiourea complex can be tuned by varying the substituent on the *N*-terminal moiety.

Experimental Section

Materials and measurements

All the chemicals and solvents were of analytical reagent grade and used without further purification. Ligands **L1**–**L5** were synthesized according to the previously reported procedure.^[19] Elemental analyses was carried out on a PerkinElmer instrument. UV/Vis spectra were recorded on a Shimadzu UV2600 spectrophotometer. FTIR spectra were recorded as KBr pellets using a Thermo Scientific Nicolet iS5 spectrometer. ¹H and ¹³C NMR spectra were recorded on a Bruker 500 MHz spectrometer. Mass spectra were recorded on a Thermo Exactive Plus UHPLC-MS spectrometer. A Bruker Quest X-ray (fixed-Chi geometry) diffractometer was employed for crystal screening, unit cell determination and data collection. The goniometer was controlled using the APEX3 software suite. Olex2 was employed for the final data presentation and structure plots.^[64–68] All the other methods related to the kinetic and biological studies are described in the Supporting Information.

Deposition Numbers 1986311 (for **C1**), 1986316 (for **C2**), 1986315 (for **C3**), 1986313 (for **C4**), 1986317 (for **C6**), 1986310 (for **C8**), and 1986312 (for **C14**) contain the supplementary crystallographic data for this paper. These data are provided free of charge by the joint Cambridge Crystallographic Data Centre and Fachinformationszentrum Karlsruhe Access Structures service www.ccdc.cam.ac.uk/structures.

Synthesis of the ligands

The ligands were synthesized according to the reported procedure with slight modifications.^[15,16,19] Fuoyl chloride (1.3052 g, 10 mmol) was added dropwise to a solution of potassium thiocyanate (0.971 g, 10 mmol) in acetone (15 mL), and the mixture was heated at reflux for 1 h. After cooling, a solution of the desired amine (0.931–2.29 g, 10 mmol; aniline (**L1**), benzylamine (**L2**), 2-phenylethanamine (**L3**), 2,6-diethylaniline (**L4**), 2,4,6-trimethylaniline (**L5**), 4-(trifluoromethyl)aniline (**L6**) or 3,5-bis(trifluoromethyl)aniline (**L7**)) in acetone (10 mL) was added dropwise to the mixture, which was stirred at room temperature for 3 h. The resulting solution was poured into 1 N HCl to neutralize any excess amine, and the solid product was filtered and washed with water to remove any traces of KCl. All the ligands were obtained in good yields of 80–90%.

N-[[4-(Trifluoromethyl)phenyl]carbamothioyl]furan-2-carboxamide (**L6**)

Yield: 82%; m.p. 135 °C; colorless; ¹H NMR (500 MHz, [D₆]DMSO): δ = 12.50 (s, 1H; OC-NH), 11.45 (s, 1H; SC-NH), 8.10 (s, 1H; aromatic), 7.95 (d, *J* = 8.3 Hz, 2H; aromatic), 7.88 (d, *J* = 3.0 Hz, 1H; aromatic), 7.79 (d, *J* = 8.4 Hz, 2H; aromatic), 6.78 ppm (dd, *J* = 3.5, 1.7 Hz, 1H; aromatic); ¹³C NMR (125 MHz, [D₆]DMSO): δ = 179.5 (C=S), 157.9 (C=O), 149.0, 145.1, 142.1, 126.8, 125.1, 123.5, 119.3, 113.2 (aromatic), 126.3, 126.3, 126.2, 126.2 ppm (CF₃); ¹⁹F NMR (471 MHz, [D₆]DMSO): δ = 60.7 ppm; UV/Vis (CHCl₃): λ_{max} (ε) = 285 (20 094), 310 nm (8333 dm³ mol⁻¹ cm⁻¹); FTIR (KBr): ν̄ = 3240 (m, ν(thioamide N–H)), 3027 (m, ν(amide N–H)), 1672 (s, ν(C=O)), 1230 cm⁻¹ (s, ν(C=S)); elemental analysis calcd (%) for C₁₃H₉F₃N₂O₂S (314.0336): C 49.68, H 2.89, N 8.91, S 10.20; found: C 49.81, H 2.74, N 8.99, S 10.32.

N-[[3,5-Bis(trifluoromethyl)phenyl]carbamothioyl]furan-2-carboxamide (**L7**)

Yield: 86%; m.p. 161 °C; colorless; ¹H NMR (500 MHz, [D₆]DMSO): δ = 12.53 (s, 1H; OC-NH), 11.62 (s, 1H; SC-NH), 8.43 (s, 2H; aromatic), 8.10 (s, 1H; aromatic), 7.98 (s, 1H; aromatic), 7.90 (d, *J* = 3.5 Hz, 1H; aromatic), 6.78 ppm (dd, *J* = 3.6, 1.8 Hz, 1H; aromatic); ¹³C NMR (125 MHz, CDCl₃): δ = 178.4 (C=S), 156.9 (C=O), 146.8, 144.5, 139.1, 132.4, 132.1, 123.8, 119.7, 113.6 (aromatic), 120.0, 120.0, 120.0, 119.9 ppm (CF₃); ¹⁹F NMR (471 MHz, [D₆]DMSO): δ = 61.5 ppm; UV/Vis (CHCl₃): λ_{max} (ε) = 286 (24 620), 317 nm (7963 dm³ mol⁻¹ cm⁻¹); FTIR (KBr): ν̄ = 3271 (m, ν(thioamide N–H)), 3117 (m, ν(amide N–H)), 1677 (s, ν(C=O)), 1230 cm⁻¹ (s, ν(C=S)); elemental analysis calcd (%) for C₁₄H₈F₆N₂O₂S (382.0210): C 43.99, H 2.11, N 7.33, S 8.39; found: C 43.75, H 2.27, N 7.21, S 8.46.

Synthesis of the Ru-*p*-cymene and Ru-benzene complexes **C1**–**C14**

The metal precursors, namely Ru-*p*-cymene and Ru-benzene dimers, required for the preparation of the complexes, were prepared according to the reported procedures.^[17–19] To prepare the complexes, the metal precursor (0.1 mmol, 500–612 mg) was added to toluene (10 mL) and the mixture stirred for a few minutes. A few drops of methanol were then added to promote the solubility of the precursor.^[19] A solution of the ligand (0.2 mmol, 493–765 mg) in toluene (10 mL) was then added dropwise. The resulting mixture was stirred for 4 h to achieve completion of the reaction, after which it was reduced in volume, and the solid product was obtained by the addition of hexane. The solid was then filtered and washed with hexane. The complexes were obtained in good yields of 70–79%.

[Dichloro(*p*-cymene){*N*-(phenylcarbamothioyl)furan-2-carboxamide}ruthenium(II)] (**C1**)

L1 (49 mg, 0.2 mmol) and [RuCl₂(*p*-cymene)]₂ (61 mg, 0.1 mmol) were used. Yield: 75%; m.p. 180 °C; orange; ¹H NMR (500 MHz, [D₆]DMSO): δ = 12.36 (s, 1H; OC-NH), 11.28 (s, 1H; SC-NH), 8.08 (d, *J* = 1.0 Hz, 1H; aromatic), 7.86 (d, *J* = 3.5 Hz, 1H; aromatic), 7.67 (d, *J* = 7.8 Hz, 2H; aromatic), 7.42 (q, *J* = 7.9 Hz, 2H; aromatic), 7.27 (t, *J* = 7.4 Hz, 1H; aromatic), 6.77 (dd, *J* = 3.6, 1.7 Hz, 1H; aromatic), 5.82 (d, *J* = 6.3 Hz, 2H; aromatic-H of *p*-cymene), 5.78 (d, *J* = 6.3 Hz, 2H; aromatic-H of *p*-cymene), 2.86–2.81 (m, 1H; CH(CH₃)₂ of *p*-cymene), 2.09 (s, 3H; C-CH₃ of *p*-cymene), 1.19 ppm (d, *J* = 6.9 Hz, 6H; CH(CH₃)₂ of *p*-cymene); ¹³C NMR (125 MHz, [D₆]DMSO): δ = 179.1 (C=S), 158.0 (C=O), 148.9, 145.1, 138.4, 129.1, 126.8, 124.8, 119.1, 113.1 (aromatic), 106.8, 100.5, 86.8, 85.9 (aromatic-C of *p*-cymene), 30.4, 21.9, 18.3 ppm (aliphatic-C of *p*-cymene); UV/Vis (CHCl₃): λ_{max} (ε) = 288 (22 580), 366 (6082), 433 nm (1290 dm³ mol⁻¹ cm⁻¹); FTIR (KBr): ν̄ = 3232 (m, ν(thioamide N–H)), 3171 (m, ν(amide N–H)), 1678 (s, ν(C=O)), 1178 cm⁻¹ (s, ν(C=S)); MS (ESI): *m/z* calcd for [C₂₂H₂₃N₂O₂RuS]⁺: 481.0524 [*M* – 2H⁺ – 2Cl⁻ + H⁺]⁺; found: 481.0538; elemental analysis calcd (%) for C₂₂H₂₄Cl₂N₂O₂RuS: C 47.83, H 4.38, N 5.07, S 5.80; found: C 47.98, H 4.51, N 5.21, S 5.61.

[Dichloro(*p*-cymene){*N*-(benzylcarbamothioyl)furan-2-carboxamide}ruthenium(II)] (**C2**)

L2 (52 mg, 0.2 mmol) and [RuCl₂(*p*-cymene)]₂ (61 mg, 0.1 mmol) were used. Yield: 72%; m.p. 196 °C; orange; ¹H NMR (500 MHz, CDCl₃): δ = 11.23 (s, 1H; OC-NH), 10.86 (s, 1H; SC-NH), 7.93 (d, *J* = 3.4 Hz, 1H; aromatic), 7.60 (s, 1H; aromatic), 7.41–7.32 (m, 5H; aro-

matic), 6.51–6.48 (m, 1H; aromatic), 5.47 (d, $J=5.7$ Hz, 2H; aromatic-H of *p*-cymene), 5.30 (d, $J=5.7$ Hz, 2H; aromatic-H of *p*-cymene), 4.86 (d, $J=5.0$ Hz, 2H; CH_2), 3.06–2.96 (m, 1H; $\text{CH}(\text{CH}_3)_2$ of *p*-cymene), 2.29 (s, 3H; $\text{C}-\text{CH}_3$ of *p*-cymene), 1.34 ppm (d, $J=6.9$ Hz, 6H; $\text{CH}(\text{CH}_3)_2$ of *p*-cymene); ^{13}C NMR (125 MHz, CDCl_3): $\delta=179.2$ (C=S), 158.7 (C=O), 147.8, 144.6, 134.9, 129.0, 128.3, 127.8, 121.5, 112.6 (aromatic), 103.5, 100.0, 84.2, 82.6 (aromatic-C of *p*-cymene), 49.5 (CH_2), 30.4, 22.2, 18.4 ppm (aliphatic-C of *p*-cymene); UV/Vis (CHCl_3): λ_{max} (ϵ)=282 (16383), 323 (4874), 429 nm ($1062 \text{ dm}^3 \text{ mol}^{-1} \text{ cm}^{-1}$); FTIR (KBr): $\tilde{\nu}=3244$ (m, ν (thioamide N–H)), 3179 (m, ν (amide N–H)), 1679 (s, ν (C=O)), 1202 cm^{-1} (s, ν (C=S)); MS (ESI): m/z calcd for $[\text{C}_{23}\text{H}_{25}\text{N}_2\text{O}_2\text{RuS}]^+$: 495.0680 [$M-2\text{H}^+-2\text{Cl}^-+\text{H}^+$] $^+$; found: 495.0656; elemental analysis calcd (%) for $\text{C}_{23}\text{H}_{26}\text{Cl}_2\text{N}_2\text{O}_2\text{RuS}$: C 48.76, H 4.63, N 4.95, S 5.66; found: C 48.59, H 4.80, N 4.81, S 5.73.

[Dichloro(*p*-cymene){*N*-(phenethylcarbamothioyl)furan-2-carboxamide}ruthenium(II)] (C3)

L3 (54 mg, 0.2 mmol) and $[\text{RuCl}_2(\textit{p}\text{-cymene})_2]$ (61 mg, 0.1 mmol) were used. Yield: 71%; m.p. 184 °C; orange; ^1H NMR (500 MHz, CDCl_3): $\delta=10.97$ (s, 1H; OC-NH), 10.74 (s, 1H; SC-NH), 7.92 (d, $J=3.2$ Hz, 1H; aromatic), 7.60 (s, 1H; aromatic), 7.36 (t, $J=7.3$ Hz, 2H; aromatic), 7.26 (d, $J=7.6$ Hz, 3H; aromatic), 6.49 (dd, $J=2.7$, 1.1 Hz, 1H; aromatic), 5.46 (d, $J=4.2$ Hz, 2H; aromatic-H of *p*-cymene), 5.29 (d, $J=3.6$ Hz, 2H; aromatic-H of *p*-cymene), 3.92 (dd, $J=12.6$, 7.6 Hz, 2H; HN- CH_2CH_2), 3.03 (t, $J=7.4$ Hz, 2H; HN- CH_2CH_2), 2.29 (s, 3H; $\text{C}-\text{CH}_3$ of *p*-cymene), 1.77–1.53 (m, 1H; $\text{CH}(\text{CH}_3)_2$ of *p*-cymene), 1.35 ppm (d, $J=6.4$ Hz, 6H; $\text{CH}(\text{CH}_3)_2$ of *p*-cymene); ^{13}C NMR (125 MHz, CDCl_3): $\delta=179.0$ (C=S), 158.6 (C=O), 147.7, 144.6, 137.4, 128.9, 128.7, 127.0, 121.4, 112.6 (aromatic), 103.4, 99.9, 84.2, 82.6 (aromatic-C of *p*-cymene), 46.9, 34.4 (CH_2CH_2), 30.4, 22.2, 18.3 ppm (aliphatic-C of *p*-cymene); UV/Vis (CHCl_3): λ_{max} (ϵ)=282 (21313), 326 (6332), 428 nm ($1351 \text{ dm}^3 \text{ mol}^{-1} \text{ cm}^{-1}$); FTIR (KBr): $\tilde{\nu}=3218$ (m, ν (thioamide N–H)), 3169 (m, ν (amide N–H)), 1668 (s, ν (C=O)), 1197 cm^{-1} (s, ν (C=S)); MS (ESI): m/z calcd for $[\text{C}_{24}\text{H}_{28}\text{Cl}_2\text{N}_2\text{O}_2\text{RuS}]^+$: 509.0836 [$M-2\text{H}^+-2\text{Cl}^-+\text{H}^+$] $^+$; found: 509.0740; elemental analysis calcd (%) for $\text{C}_{24}\text{H}_{28}\text{Cl}_2\text{N}_2\text{O}_2\text{RuS}$: C 49.52, H 4.95, N 4.77, S 5.46; found: C 49.66, H 4.83, N 4.92, S 5.60.

[Dichloro(*p*-cymene){*N*-{(2,6-diethylphenyl)carbamothioyl}-furan-2-carboxamide}ruthenium(II)] (C4)

L4 (60 mg, 0.2 mmol) and $[\text{RuCl}_2(\textit{p}\text{-cymene})_2]$ (61 mg, 0.1 mmol) were used. Yield: 72%; m.p. 210 °C; orange; ^1H NMR (500 MHz, CDCl_3): $\delta=12.08$ (s, 1H; OC-NH), 11.17 (s, 1H; SC-NH), 8.05 (d, $J=4.2$ Hz, 1H; aromatic), 7.65 (s, 1H; aromatic), 7.36 (t, $J=8.1$ Hz, 1H; aromatic), 7.21 (d, $J=8.3$ Hz, 2H; aromatic), 6.54 (dd, $J=3.8$, 1.5 Hz, 1H; aromatic), 5.32 (d, $J=6.5$ Hz, 2H; aromatic-H of *p*-cymene), 5.21 (d, $J=6.5$ Hz, 2H; aromatic-H of *p*-cymene), 2.89–2.79 (m, 1H; $\text{CH}(\text{CH}_3)_2$ of *p*-cymene), 2.67–2.58 (m, 4H; CH_2CH_3), 2.21 (s, 3H; $\text{C}-\text{CH}_3$ of *p*-cymene), 1.25–1.19 ppm (m, 12H; $\text{CH}(\text{CH}_3)_2$ of *p*-cymene, CH_2CH_3); ^{13}C NMR (125 MHz, CDCl_3): $\delta=181.5$ (C=S), 159.0 (C=O), 147.9, 144.7, 141.3, 133.32, 129.1, 126.6, 121.9, 112.7 (aromatic), 103.0, 99.8, 83.8, 82.8 (aromatic-C of *p*-cymene), 24.7, 14.3 (CH_2CH_3), 30.2, 22.0, 18.2 ppm (aliphatic-C of *p*-cymene); UV/Vis (CHCl_3): λ_{max} (ϵ)=283 (17553), 342 (4645), 428 nm ($1099 \text{ dm}^3 \text{ mol}^{-1} \text{ cm}^{-1}$); FTIR (KBr): $\tilde{\nu}=3215$ (m, ν (thioamide N–H)), 3129 (m, ν (amide N–H)), 1664 (s, ν (C=O)), 1168 cm^{-1} (s, ν (C=S)); MS (ESI): m/z calcd for $[\text{C}_{26}\text{H}_{31}\text{N}_2\text{O}_2\text{RuS}]^+$: 537.1149 [$M-2\text{H}^+-2\text{Cl}^-+\text{H}^+$] $^+$; found: 537.1052; elemental analysis calcd (%) for $\text{C}_{26}\text{H}_{32}\text{Cl}_2\text{N}_2\text{O}_2\text{RuS}$: C 51.31, H 5.30, N 4.60, S 5.27; found: C 51.45, H 5.18, N 4.72, S 5.45.

[Dichloro(*p*-cymene){*N*-(mesitylcarbamothioyl)furan-2-carboxamide}ruthenium(II)] (C5)

L5 (57 mg, 0.2 mmol) and $[\text{RuCl}_2(\textit{p}\text{-cymene})_2]$ (61 mg, 0.1 mmol) were used. Yield: 76%; m.p. 197 °C; orange; ^1H NMR (500 MHz, $[\text{D}_6]\text{DMSO}$): $\delta=11.60$ (s, 1H; OC-NH), 11.30 (s, 1H; SC-NH), 8.07 (d, $J=1.5$ Hz, 1H; aromatic), 7.86 (d, $J=3.6$ Hz, 1H; aromatic), 6.93 (s, 2H; aromatic), 6.77 (dd, $J=3.6$, 1.7 Hz, 1H; aromatic), 5.82 (d, $J=6.3$ Hz, 2H; aromatic-H of *p*-cymene), 5.78 (d, $J=6.3$ Hz, 2H; aromatic-H of *p*-cymene), 2.90–2.76 (m, 1H; $\text{CH}(\text{CH}_3)_2$ of *p*-cymene), 2.25 (s, 3H; $\text{C}-\text{CH}_3$ of *p*-cymene), 2.14 (s, 6H; $\text{o}-\text{CH}_3$), 2.09 ppm (s, 3H; $\text{p}-\text{CH}_3$), 1.20 ppm (d, $J=6.9$ Hz, 6H; $\text{CH}(\text{CH}_3)_2$ of *p*-cymene); ^{13}C NMR (125 MHz, $[\text{D}_6]\text{DMSO}$): $\delta=180.4$ (C=S), 157.9 (C=O), 148.8, 145.2, 137.0, 135.1, 134.1, 129.3, 118.9, 113.1 (aromatic), 106.8, 100.5, 86.8, 85.9 (aromatic-C of *p*-cymene), 30.4, 21.9, 18.2 (aliphatic-C of *p*-cymene), 21.0, 18.3 ppm ($\text{o},\text{p}-\text{CH}_3$); UV/Vis (CHCl_3): λ_{max} (ϵ)=285 (15823), 346 (7685), 433 nm ($1062 \text{ dm}^3 \text{ mol}^{-1} \text{ cm}^{-1}$); FTIR (KBr): $\tilde{\nu}=3226$ (m, ν (thioamide N–H)), 3115 (m, ν (amide N–H)), 1671 (s, ν (C=O)), 1184 cm^{-1} (s, ν (C=S)); MS (ESI): m/z calcd for $[\text{C}_{25}\text{H}_{29}\text{N}_2\text{O}_2\text{RuS}]^+$: 523.0993 [$M-2\text{H}^+-2\text{Cl}^-+\text{H}^+$] $^+$; found: 523.1011; elemental analysis calcd (%) for $\text{C}_{25}\text{H}_{30}\text{Cl}_2\text{N}_2\text{O}_2\text{RuS}$: C 50.50, H 5.09, N 4.71, S 5.39; found: C 50.67, H 5.24, N 4.54, S 5.51.

[Dichloro(*p*-cymene){*N*-{(4-(trifluoromethyl)phenyl)carbamothioyl)furan-2-carboxamide}ruthenium(II)] (C6)

L6 (62 mg, 0.2 mmol) and $[\text{RuCl}_2(\textit{p}\text{-cymene})_2]$ (61 mg, 0.1 mmol) were used. Yield: 79%; m.p. 181 °C; orange; ^1H NMR (500 MHz, $[\text{D}_6]\text{DMSO}$): $\delta=12.50$ (s, 1H; OC-NH), 11.46 (s, 1H; SC-NH), 8.10 (s, 1H; aromatic), 7.95 (d, $J=8.3$ Hz, 2H; aromatic), 7.88 (d, $J=3.5$ Hz, 1H; aromatic), 7.79 (d, $J=8.3$ Hz, 2H; aromatic), 6.78 (dd, $J=3.9$, 1.8 Hz, 1H; aromatic), 5.82 (d, $J=6.2$ Hz, 2H; aromatic-H of *p*-cymene), 5.78 (d, $J=6.1$ Hz, 2H; aromatic-H of *p*-cymene), 2.89–2.78 (m, 1H; $\text{CH}(\text{CH}_3)_2$ of *p*-cymene), 2.09 (s, 3H; $\text{C}-\text{CH}_3$ of *p*-cymene), 1.20 ppm (d, $J=6.9$ Hz, 6H; $\text{CH}(\text{CH}_3)_2$ of *p*-cymene); ^{13}C NMR (125 MHz, $[\text{D}_6]\text{DMSO}$): $\delta=179.5$ (C=S), 157.9 (C=O), 149.0, 145.1, 142.1, 126.8, 125.1, 123.4, 119.3, 113.1 (aromatic), 126.3, 126.2, 126.2, 126.2 (CF_3), 106.8, 100.5, 86.8, 85.9 (aromatic-C of *p*-cymene), 30.4, 21.9, 18.3 ppm (aliphatic-C of *p*-cymene); ^{19}F NMR (471 MHz, $[\text{D}_6]\text{DMSO}$): $\delta=60.7$ ppm; UV/Vis (CHCl_3): λ_{max} (ϵ)=291 (15780), 359 (3561), 428 nm ($849 \text{ dm}^3 \text{ mol}^{-1} \text{ cm}^{-1}$); FTIR (KBr): $\tilde{\nu}=3149$ (m, ν (thioamide N–H)), 3031 (m, ν (amide N–H)), 1678 (s, ν (C=O)), 1172 cm^{-1} (s, ν (C=S)); MS (ESI): m/z calcd for $[\text{C}_{25}\text{H}_{22}\text{F}_3\text{N}_2\text{O}_2\text{RuS}]^+$: 549.0397 [$M-2\text{H}^+-2\text{Cl}^-+\text{H}^+$] $^+$; found: 549.0314; elemental analysis calcd (%) for $\text{C}_{25}\text{H}_{23}\text{Cl}_2\text{F}_3\text{N}_2\text{O}_2\text{RuS}$: C 44.52, H 3.74, N 4.51, S 5.17; found: C 44.69, H 3.90, N 4.37, S 5.34.

[Dichloro(*p*-cymene){*N*-{(3,5-bis(trifluoromethyl)phenyl)carbamothioyl)furan-2-carboxamide}ruthenium(II)] (C7)

L7 (76 mg, 0.2 mmol) and $[\text{RuCl}_2(\textit{p}\text{-cymene})_2]$ (61 mg, 0.1 mmol) were used. Yield: 77%; m.p. 185 °C; orange; ^1H NMR (500 MHz, $[\text{D}_6]\text{DMSO}$): $\delta=12.51$ (s, 1H; OC-NH), 11.64 (s, 1H; SC-NH), 8.43 (s, 2H; aromatic), 8.11 (d, $J=0.9$ Hz, 1H; aromatic), 8.01 (s, 1H; aromatic), 7.90 (d, $J=3.5$ Hz, 1H; aromatic), 6.79 (dd, $J=3.6$, 1.6 Hz, 1H; aromatic), 5.83 (d, $J=6.2$ Hz, 2H; aromatic-H of *p*-cymene), 5.79 (d, $J=6.2$ Hz, 2H; aromatic-H of *p*-cymene), 2.89–2.79 (m, 1H; $\text{CH}(\text{CH}_3)_2$ of *p*-cymene), 2.09 (s, 3H; $\text{C}-\text{CH}_3$ of *p*-cymene), 1.20 ppm (d, $J=6.9$ Hz, 6H; $\text{CH}(\text{CH}_3)_2$ of *p*-cymene); ^{13}C NMR (125 MHz, $[\text{D}_6]\text{DMSO}$): $\delta=180.4$ (C=S), 157.7 (C=O), 149.2, 145.0, 140.6, 130.9, 130.6, 124.6, 119.4, 113.2 (aromatic), 120.0, 119.9 (CF_3), 106.8, 100.5, 86.8, 85.9 (aromatic-C of *p*-cymene), 30.4, 21.9, 18.3 ppm (aliphatic-C of *p*-cymene); ^{19}F NMR (471 MHz, $[\text{D}_6]\text{DMSO}$): $\delta=61.4$ ppm; UV/Vis (CHCl_3): λ_{max} (ϵ)=292 (19260), 364 (4260), 429 nm

(985 dm³ mol⁻¹ cm⁻¹); FTIR (KBr): $\tilde{\nu}$ = 3228 (m, ν (thioamide N–H)), 3118 (m, ν (amide N–H)), 1683 (s, ν (C=O)), 1180 cm⁻¹ (s, ν (C=S)); MS (ESI): m/z calcd for [C₂₄H₂₁F₆N₂O₂RuS]⁺: 617.0271 [M–2H⁺–2Cl⁻+H⁺]⁺; found: 617.0297; elemental analysis calcd (%) for C₂₄H₂₂Cl₂F₆N₂O₂RuS: C 41.87, H 3.22, N 4.07, S 4.66; found: C 41.68, H 3.41, N 4.20, S 4.85.

[Dichloro(benzene){N-(phenylcarbamothioyl)furan-2-carboxamide}ruthenium(II)] (C8)

L1 (49 mg, 0.2 mmol) and [RuCl₂(benzene)]₂ (50 mg, 0.1 mmol) were used. Yield: 74%; m.p. 250 °C; orange; ¹H NMR (500 MHz, [D₆]DMSO): δ = 12.34 (s, 1H; OC-NH), 11.27 (s, 1H; SC-NH), 8.07 (d, J = 1.0 Hz, 1H; aromatic), 7.85 (d, J = 3.6 Hz, 1H; aromatic), 7.65 (d, J = 8.9 Hz, 2H; aromatic), 7.41 (t, J = 8.1 Hz, 2H; aromatic), 7.26 (t, J = 7.6 Hz, 1H; aromatic), 6.75 (dd, J = 3.8, 1.8 Hz, 1H; aromatic), 5.96 ppm (s, 6H; aromatic-H of benzene); ¹³C NMR (125 MHz, [D₆]DMSO): δ = 179.1 (C=S), 158.0 (C=O), 148.9, 145.1, 138.4, 129.1, 126.8, 124.8, 119.1, 113.1 (aromatic), 88.1 ppm (aromatic-C of benzene); UV/Vis (CHCl₃): λ_{max} (ϵ) = 289 (25888), 362 (6380), 424 nm (1500 dm³ mol⁻¹ cm⁻¹); FTIR (KBr): $\tilde{\nu}$ = 3229 (m, ν (thioamide N–H)), 3159 (m, ν (amide N–H)), 1672 (s, ν (C=O)), 1182 cm⁻¹ (s, ν (C=S)); MS (ESI): m/z calcd for [C₁₈H₁₅N₂O₂RuS]⁺: 424.9898 [M–2H⁺–2Cl⁻+H⁺]⁺; found: 424.9902; elemental analysis calcd (%) for C₁₈H₁₆Cl₂N₂O₂RuS: C 43.56, H 3.25, N 5.64, S 6.46; found: C 43.71, H 3.04, N 5.42, S 6.64.

[Dichloro(benzene){N-(benzylcarbamothioyl)furan-2-carboxamide}ruthenium(II)] (C9)

L2 (52 mg, 0.2 mmol) and [RuCl₂(benzene)]₂ (50 mg, 0.1 mmol) were used. Yield: 70%; m.p. 242 °C; orange; ¹H NMR (500 MHz, CDCl₃): δ = 11.06 (s, 1H; OC-NH), 10.93 (s, 1H; SC-NH), 7.97 (d, J = 1.6 Hz, 1H; aromatic), 7.73 (d, J = 3.5 Hz, 1H; aromatic), 7.30 (s, 2H; aromatic), 7.29 (d, J = 3.3 Hz, 2H; aromatic), 7.22 (dt, J = 8.2, 4.1 Hz, 1H; aromatic-H), 6.66 (dd, J = 3.4, 1.5 Hz, 1H; aromatic), 5.90 (s, 6H; aromatic-H of benzene), 4.79 ppm (d, J = 5.7 Hz, 2H; CH₂); ¹³C NMR (125 MHz, CDCl₃): δ = 185.3 (C=S), 162.6 (C=O), 149.9, 142.1, 133.5, 132.6, 132.4, 123.4, 123.3, 117.6 (aromatic), 92.8 (aromatic-C of benzene), 53.5 ppm (CH₂); UV/Vis (CHCl₃): λ_{max} (ϵ) = 284 (18403), 321 (6525), 425 nm (985 dm³ mol⁻¹ cm⁻¹); FTIR (KBr): $\tilde{\nu}$ = 3222 (m, ν (thioamide N–H)), 3131 (m, ν (amide N–H)), 1675 (s, ν (C=O)), 1201 cm⁻¹ (s, ν (C=S)); MS (ESI): m/z calcd for [C₁₉H₁₇N₂O₂RuS]⁺: 439.0054 [M–2H⁺–2Cl⁻+H⁺]⁺; found: 439.0264; elemental analysis calcd (%) for C₁₉H₁₈Cl₂N₂O₂RuS: C 44.71, H 3.55, N 5.49, S 6.28; found: C 44.53, H 3.70, N 5.65, S 6.10.

[Dichloro(benzene){N-(phenethylcarbamothioyl)furan-2-carboxamide}ruthenium(II)] (C10)

L3 (54 mg, 0.2 mmol) and [RuCl₂(benzene)]₂ (50 mg, 0.1 mmol) were used. Yield: 71%; m.p. 238 °C; orange; ¹H NMR (500 MHz, CDCl₃): δ = 10.99 (s, 1H; OC-NH), 10.67 (s, 1H; SC-NH), 7.86 (d, J = 4.2 Hz, 1H; aromatic), 7.62 (s, 1H; aromatic), 7.36 (dd, J = 8.8, 5.7 Hz, 2H; aromatic), 7.30–7.24 (m, 4H; aromatic), 6.50 (dd, J = 3.9, 1.3 Hz, 1H; aromatic), 5.73 (s, 6H; aromatic-H of benzene), 3.94 (dd, J = 12.6, 6.9 Hz, 2H; HN-CH₂CH₂), 3.03 ppm (t, J = 7.1 Hz, 2H; HN-CH₂CH₂); ¹³C NMR (125 MHz, CDCl₃): δ = 178.8 (C=S), 158.5 (C=O), 147.8, 144.5, 137.3, 128.9, 128.7, 127.1, 121.4, 112.7 (aromatic), 85.5 (aromatic-C of benzene), 47.0, 34.4 ppm (CH₂CH₂); UV/Vis (CHCl₃): λ_{max} (ϵ) = 284 (15191), 322 (6510), 430 nm (936 dm³ mol⁻¹ cm⁻¹); FTIR (KBr): $\tilde{\nu}$ = 3229 (m, ν (thioamide N–H)), 3184 (m, ν (amide N–H)), 1675 (s, ν (C=O)), 1194 cm⁻¹ (s, ν (C=S)); MS (ESI): m/z calcd for [C₂₀H₁₉N₂O₂RuS]⁺: 453.0211 [M–2H⁺–2Cl⁻+H⁺]⁺; found: 453.0150; elemental analysis calcd (%) for C₂₀H₂₀Cl₂N₂O₂RuS: C 45.81, H 3.84, N 5.34, S 6.11; found: C 45.69, H 3.97, N 5.23, S 6.26.

[Dichloro(benzene){N-(2,6-diethylphenyl)carbamothioyl}furan-2-carboxamide}ruthenium(II)] (C11)

[Dichloro(benzene){N-(2,6-diethylphenyl)carbamothioyl}furan-2-carboxamide}ruthenium(II)] (C11)

L4 (60 mg, 0.2 mmol) and [RuCl₂(benzene)]₂ (50 mg, 0.1 mmol) were used. Yield: 73%; m.p. 220 °C; orange; ¹H NMR (500 MHz, CDCl₃): δ = 12.13 (s, 1H; OC-NH), 11.12 (s, 1H; SC-NH), 7.98 (d, J = 3.4 Hz, 1H; aromatic), 7.66 (s, 1H; aromatic), 7.37 (t, J = 7.5 Hz, 1H; aromatic), 7.22 (d, J = 7.6 Hz, 2H; aromatic), 6.54 (dd, J = 3.6, 1.3 Hz, 1H; aromatic), 5.62 (s, 6H; aromatic-H of benzene), 2.66–2.59 (m, 4H; CH₂CH₃), 1.22 ppm (t, J = 7.5 Hz, 6H; CH₂CH₃); ¹³C NMR (125 MHz, CDCl₃): δ = 181.1 (C=S), 159.0 (C=O), 148.1, 144.6, 141.2, 133.0, 129.3, 126.7, 122.0, 112.8 (aromatic), 85.3 (aromatic-C of benzene), 24.8, 14.4 ppm (CH₂CH₃); UV/Vis (CHCl₃): λ_{max} (ϵ) = 284 (18996), 322 (5501), 428 nm (1003 dm³ mol⁻¹ cm⁻¹); FTIR (KBr): $\tilde{\nu}$ = 3204 (m, ν (thioamide N–H)), 3136 (m, ν (amide N–H)), 1671 (s, ν (C=O)), 1166 cm⁻¹ (s, ν (C=S)); MS (ESI): m/z calcd for [C₂₂H₂₃N₂O₂RuS]⁺: 481.0524 [M–2H⁺–2Cl⁻+H⁺]⁺; found: 481.0395; elemental analysis calcd (%) for C₂₂H₂₄Cl₂N₂O₂RuS: C 47.83, H 4.38, N 5.07, S 5.80; found: C 47.99, H 4.21, N 5.19, S 5.61.

[Dichloro(benzene){N-(mesitylcarbamothioyl)furan-2-carboxamide}ruthenium(II)] (C12)

L5 (57 mg, 0.2 mmol) and [RuCl₂(benzene)]₂ (50 mg, 0.1 mmol) were used. Yield: 76%; m.p. 248 °C; orange; ¹H NMR (500 MHz, [D₆]DMSO): δ = 11.60 (s, 1H; OC-NH), 11.33 (s, 1H; SC-NH), 8.08 (s, 1H; aromatic), 7.87 (d, J = 3.8 Hz, 1H; aromatic), 6.93 (s, 2H; aromatic), 6.77 (dd, J = 3.6, 1.6 Hz, 1H; aromatic), 5.97 (s, 6H; aromatic-H of benzene), 2.25 (s, 3H; *p*-CH₃), 2.1 ppm (s, 6H; *o*-CH₃); ¹³C NMR (125 MHz, [D₆]DMSO): δ = 180.4 (C=S), 157.9 (C=O), 148.8, 145.2, 137.0, 135.1, 134.1, 128.9, 118.9, 113.1 (aromatic), 88.1 (aromatic-C of benzene), 21.0, 18.2 ppm (*o,p*-CH₃); UV/Vis (CHCl₃): λ_{max} (ϵ) = 283 (21285), 326 (6666), 424 nm (1095 dm³ mol⁻¹ cm⁻¹); FTIR (KBr): $\tilde{\nu}$ = 3227 (m, ν (thioamide N–H)), 3143 (m, ν (amide N–H)), 1676 (s, ν (C=O)), 1185 cm⁻¹ (s, ν (C=S)); MS (ESI): m/z calcd for [C₂₁H₂₁N₂O₂RuS]⁺: 467.0367 [M–2H⁺–2Cl⁻+H⁺]⁺; found: 467.0283; elemental analysis calcd (%) for C₂₁H₂₂Cl₂N₂O₂RuS: C 46.84, H 4.12, N 5.20, S 5.95; found: C 46.67, H 4.29, N 5.35, S 5.72.

[Dichloro(benzene){N-(4-(trifluoromethyl)phenyl)carbamothioyl}furan-2-carboxamide}ruthenium(II)] (C13)

L6 (62 mg, 0.2 mmol) and [RuCl₂(benzene)]₂ (50 mg, 0.1 mmol) were used. Yield: 77%; m.p. 241 °C; orange; ¹H NMR (500 MHz, [D₆]DMSO): δ = 12.50 (s, 1H; OC-NH), 11.46 (s, 1H; SC-NH), 8.10 (s, 1H; aromatic), 7.95 (d, J = 8.3 Hz, 2H; aromatic), 7.88 (d, J = 3.5 Hz, 1H; aromatic), 7.79 (d, J = 8.4 Hz, 2H; aromatic), 6.78 (dd, J = 3.6, 1.7 Hz, 1H; aromatic), 5.98 ppm (s, 6H; aromatic-H of benzene); ¹³C NMR (125 MHz, [D₆]DMSO): δ = 179.5 (C=S), 157.9 (C=O), 149.0, 145.1, 142.1, 128.7, 126.2, 126.2, 126.2, 126.2 (CF₃), 125.1, 123.4, 119.3, 113.1 (aromatic), 88.1 ppm (aromatic-C of benzene); ¹⁹F NMR (471 MHz, [D₆]DMSO): δ = 60.5 ppm; UV/Vis (CHCl₃): λ_{max} (ϵ) = 292 (15326), 344 (4477), 426 nm (882 dm³ mol⁻¹ cm⁻¹); FTIR (KBr): $\tilde{\nu}$ = 3149 (m, ν (thioamide N–H)), 3031 (m, ν (amide N–H)), 1678 (s, ν (C=O)), 1172 cm⁻¹ (s, ν (C=S)); MS (ESI): m/z calcd for [C₁₉H₁₄F₃N₂O₂RuS]⁺: 492.9771 [M–2H⁺–2Cl⁻+H⁺]⁺; found: 492.9701; elemental analysis calcd (%) for C₁₉H₁₅Cl₂F₃N₂O₂RuS: C 40.44, H 2.68, N 4.96, S 5.68; found: C 40.62, H 2.51, N 4.77, S 5.85.

[Dichloro(benzene){N-((3,5-bis(trifluoromethyl)phenyl)carbamothioyl)furan-2-carboxamide}ruthenium(II)] (C14)

L7 (76 mg, 0.2 mmol) and $[\text{RuCl}_2(\text{benzene})_2]$ (50 mg, 0.1 mmol) were used. Yield: 78%; m.p. 230 °C; orange; $^1\text{H NMR}$ (500 MHz, $[\text{D}_6]\text{DMSO}$): $\delta = 12.36$ (s, 1H; OC-NH), 11.31 (s, 1H; SC-NH), 8.09 (s, 1H; aromatic), 7.87 (d, $J = 4.2$ Hz, 1H; aromatic), 7.67 (d, $J = 9.0$ Hz, 2H; aromatic), 7.28 (t, $J = 7.8$ Hz, 1H; aromatic), 6.77 (dd, $J = 3.9$, 1.8 Hz, 1H; aromatic), 5.98 ppm (s, 6H; aromatic-H of benzene); $^{13}\text{C NMR}$ (125 MHz, $[\text{D}_6]\text{DMSO}$): $\delta = 179.1$ (C=S), 158.0 (C=O), 148.9, 145.1, 138.4, 129.1, 126.8, 124.8, 119.1, 113.1 (aromatic), 88.1 ppm (aromatic-C of benzene); $^{19}\text{F NMR}$ (471 MHz, $[\text{D}_6]\text{DMSO}$): $\delta = 61.4$ ppm; UV/Vis (CHCl_3): λ_{max} (ϵ) = 292 (19476), 349 (4809), 423 nm ($952 \text{ dm}^3 \text{ mol}^{-1} \text{ cm}^{-1}$); FTIR (KBr): $\tilde{\nu} = 3221$ (m, $\nu(\text{thioamide N-H})$), 3114 (m, $\nu(\text{amide N-H})$), 1675 (s, $\nu(\text{C=O})$), 1181 cm^{-1} (s, $\nu(\text{C=S})$); MS (ESI): m/z calcd for $[\text{C}_{20}\text{H}_{13}\text{F}_6\text{N}_2\text{O}_2\text{RuS}]^+$: 560.9645 [$M-2\text{H}^+ - 2\text{Cl}^- + \text{H}^+$] $^+$; found: 560.9841; elemental analysis calcd (%) for $\text{C}_{20}\text{H}_{14}\text{Cl}_2\text{F}_6\text{N}_2\text{O}_2\text{RuS}$: C 37.99, H 2.23, N 4.43, S 5.07; found: C 38.15, H 2.13, N 4.59, S 5.21.

Acknowledgements

S.S. thanks the Department of Science and Technology, Ministry of Science and Technology, Government of India, for a doctoral fellowship under the DST-INSPIRE (IF160449) programme. R.K. gratefully acknowledges SERB (EMR/2016/003215) for financial support.

Conflict of interest

The authors declare no conflict of interest.

Keywords: antitumor agents • apoptosis • biological activity • ligand effects • ruthenium arene

- R. G. Kenny, C. J. Marmion, *Chem. Rev.* **2019**, *119*, 1058–1137.
- S. Komeda, H. Yoneyama, M. Uemura, A. Muramatsu, N. Okamoto, H. Konishi, H. Takahashi, A. Takagi, W. Fukuda, T. Imanaka, T. Kanbe, S. Harusawa, Y. Yoshikawa, K. Yoshikawa, *Inorg. Chem.* **2017**, *56*, 802–811.
- V. Koch, A. Meschkov, W. Feuerstein, J. Pfeifer, O. Fuhr, M. Nieger, U. Schepers, S. Bräse, *Inorg. Chem.* **2019**, *58*, 15917–15926.
- L. Zeng, P. Gupta, Y. Chen, E. Wang, L. Ji, H. Chao, Z. S. Chen, *Chem. Soc. Rev.* **2017**, *46*, 5771–5804.
- S. M. Meier-Menches, C. Gerner, W. Berger, C. G. Hartinger, B. K. Keppler, *Chem. Soc. Rev.* **2018**, *47*, 909–928.
- M. Rausch, P. J. Dyson, P. Nowak-Sliwinski, *Adv. Ther.* **2019**, *2*, 1900042.
- N. Balakrishnan, J. Haribabu, D. A. Krishnan, S. Swaminathan, D. Mahendiran, N. S. P. Bhuvanesh, R. Karvembu, *Polyhedron* **2019**, *170*, 188–201.
- N. Balakrishnan, J. Haribabu, A. K. Dhanabalan, S. Swaminathan, S. Sun, D. F. Dibwe, N. Bhuvanesh, S. Awale, R. Karvembu, *Dalton Trans.* **2020**, *49*, 9411–9424.
- P. Vasanthakumar, D. Sindhuja, D. Senthil Raja, C.-H. Lin, R. Karvembu, *New J. Chem.* **2020**, *44*, 8223–8231.
- P. N. Sathishkumar, N. Raveendran, N. S. P. Bhuvanesh, R. Karvembu, *J. Organomet. Chem.* **2018**, *876*, 57–65.
- J. Haribabu, G. Sabapathi, M. Muthu Tamizh, C. Balachandran, N. S. P. Bhuvanesh, P. Venunalingam, R. Karvembu, *Organometallics* **2018**, *37*, 1242–1257.
- J. Haribabu, S. Srividya, R. Umamathi, D. Gayathri, P. Venkatesu, N. Bhuvanesh, R. Karvembu, *Inorg. Chem. Commun.* **2020**, *119*, 108054.
- N. Y. S. Lam, D. Truong, H. Burmeister, M. V. Babak, H. U. Holtkamp, S. Movassaghi, D. M. Ayine-Tora, A. Zafar, M. Kubanik, L. Oehninger, T. Söhnel, J. Reynisson, S. M. F. Jamieson, C. Gaiddon, I. Ott, C. G. Hartinger, *Inorg. Chem.* **2018**, *57*, 14427–14434.
- B. S. Murray, M. V. Babak, C. G. Hartinger, P. J. Dyson, *Coord. Chem. Rev.* **2016**, *306*, 86–114.
- K. Jeyalakshmi, J. Haribabu, C. Balachandran, N. S. P. Bhuvanesh, N. Emi, R. Karvembu, *New J. Chem.* **2017**, *41*, 2672–2686.
- K. Jeyalakshmi, J. Haribabu, N. S. P. Bhuvanesh, R. Karvembu, *Dalton Trans.* **2016**, *45*, 12518–12531.
- G. Rohini, J. Haribabu, K. N. Aneesrahman, N. S. P. Bhuvanesh, K. Ramiah, R. Karvembu, A. Sreekanth, *Polyhedron* **2018**, *152*, 147–154.
- G. Rohini, J. Haribabu, M. M. Sheeba, K. N. Aneesrahman, N. S. P. Bhuvanesh, C. Balachandran, R. Karvembu, A. Sreekanth, *ChemistrySelect* **2018**, *3*, 18–28.
- S. Swaminathan, J. Haribabu, N. K. Kalagatur, R. Konakanchi, N. Balakrishnan, N. Bhuvanesh, R. Karvembu, *ACS Omega* **2019**, *4*, 6245–6256.
- S. W. Chang, A. R. Lewis, K. E. Prosser, J. R. Thompson, M. Gladkikh, M. B. Bally, J. J. Warren, C. J. Walsby, *Inorg. Chem.* **2016**, *55*, 4850–4863.
- L. Guo, H. Zhang, M. Tian, Z. Tian, Y. Xu, Y. Yang, H. Peng, P. Liu, Z. Liu, *New J. Chem.* **2018**, *42*, 16183–16192.
- K. Purkait, S. Chatterjee, S. Karmakar, A. Mukherjee, *Dalton Trans.* **2016**, *45*, 8541–8555.
- A. Sarkar, S. Acharya, K. Khushvant, K. Purkait, A. Mukherjee, *Dalton Trans.* **2019**, *48*, 7187–7197.
- B. N. Cunha, L. Luna-Dulcey, A. M. Plutin, R. G. Silveira, J. Honorato, R. R. Cairo, T. D. de Oliveira, M. R. Cominetti, E. E. Castellano, A. A. Batista, *Inorg. Chem.* **2020**, *59*, 5072–5085.
- A. D. Phillips, O. Zava, R. Scopelitti, A. A. Nazarov, P. J. Dyson, *Organometallics* **2010**, *29*, 417–427.
- A. Moreno, P. S. Pregosin, G. Laurency, A. D. Phillips, P. J. Dyson, *Organometallics* **2009**, *28*, 6432–6441.
- I. Romero-Canelón, L. Salassa, P. J. Sadler, *J. Med. Chem.* **2013**, *56*, 1291–1300.
- Z. Liu, A. Habtemariam, A. M. Pizarro, S. A. Fletcher, A. Kisova, O. Vrana, L. Salassa, P. C. A. Bruijninx, G. J. Clarkson, V. Brabec, P. J. Sadler, *J. Med. Chem.* **2011**, *54*, 3011–3026.
- J. Zhao, S. Li, X. Wang, G. Xu, S. Gou, *Inorg. Chem.* **2019**, *58*, 2208–2217.
- E. Namiecińska, B. Sadowska, M. Więckowska-Szakiel, A. Dołęga, B. Pasternak, M. Grażul, E. Budzisz, *RSC Adv.* **2019**, *9*, 38629–38645.
- K. Jeyalakshmi, J. Haribabu, C. Balachandran, S. Swaminathan, N. Bhuvanesh, R. Karvembu, *Organometallics* **2019**, *38*, 753–770.
- J. Haribabu, C. Balachandran, M. M. Tamizh, Y. Arun, N. S. P. Bhuvanesh, S. Aoki, R. Karvembu, *J. Inorg. Biochem.* **2020**, *205*, 110988.
- M. Tian, J. Li, S. Zhang, L. Guo, X. He, D. Kong, H. Zhang, Z. Liu, *Chem. Commun.* **2017**, *53*, 12810–12813.
- Z. Xu, D. Kong, X. He, L. Guo, X. Ge, X. Liu, H. Zhang, J. Li, Y. Yang, Z. Liu, *Inorg. Chem. Front.* **2018**, *5*, 2100–2105.
- R. Li, Y. Ma, X. Hu, W. Wu, X. Wu, C. Dong, S. Shi, Y. Lin, *Dalton Trans.* **2020**, *49*, 8864–8871.
- S. Balaji, M. K. M. Subarkhan, R. Ramesh, H. Wang, D. Semeril, *Organometallics* **2020**, *39*, 1366–1375.
- F. Wang, A. Habtemariam, E. P. L. Van Der Geer, R. Fernández, M. Melchart, R. J. Deeth, R. Aird, S. Guichard, F. P. A. Fabbiani, P. Lozano-Casal, I. D. H. Oswald, D. I. Jodrell, S. Parsons, P. J. Sadler, *Proc. Natl. Acad. Sci. USA* **2005**, *102*, 18269–18274.
- A. Rilak Simović, R. Masnikosa, I. Bratsos, E. Alessio, *Coord. Chem. Rev.* **2019**, *398*, 113011.
- A. E. Egger, C. G. Hartinger, A. K. Renfrew, P. J. Dyson, *J. Biol. Inorg. Chem.* **2010**, *15*, 919–927.
- A. K. Renfrew, A. D. Phillips, E. Tapavicza, R. Scopelitti, U. Rothlisberger, P. J. Dyson, *Organometallics* **2009**, *28*, 5061–5071.
- C. Scolaro, C. G. Hartinger, C. S. Allardyce, B. K. Keppler, P. J. Dyson, *J. Inorg. Biochem.* **2008**, *102*, 1743–1748.
- F. Wang, H. Chen, S. Parsons, I. D. H. Oswald, J. E. Davidson, P. J. Sadler, *Chem. Eur. J.* **2003**, *9*, 5810–5820.
- M. Melchart, A. Habtemariam, O. Novakova, S. A. Moggach, F. P. A. Fabbiani, S. Parsons, V. Brabec, P. J. Sadler, *Inorg. Chem.* **2007**, *46*, 8950–8962.
- S. J. Dougan, M. Melchart, A. Habtemariam, S. Parsons, P. J. Sadler, *Inorg. Chem.* **2006**, *45*, 10882–10894.
- P. Štarha, L. Hanousková, Z. Trávníček, *PLoS One* **2015**, *10*, e0143871.

- [46] Z. Liu, I. Romero-Canelón, B. Qamar, J. M. Hearn, A. Habtemariam, N. P. E. Barry, A. M. Pizarro, G. J. Clarkson, P. J. Sadler, *Angew. Chem. Int. Ed.* **2014**, *53*, 3941–3946; *Angew. Chem.* **2014**, *126*, 4022–4027.
- [47] A. Mukherjee, S. Acharya, K. Purkait, K. Chakraborty, A. Bhattacharjee, A. Mukherjee, *Inorg. Chem.* **2020**, *59*, 6581–6594.
- [48] F. Wang, J. Xu, A. Habtemariam, J. Bella, P. J. Sadler, *J. Am. Chem. Soc.* **2005**, *127*, 17734–17743.
- [49] F. Wang, J. Xu, K. Wu, S. K. Weidt, C. L. Mackay, P. R. R. Langridge-Smith, P. J. Sadler, *Dalton Trans.* **2013**, *42*, 3188–3195.
- [50] A. Chatterjee, *Nutrients* **2013**, *5*, 525–542.
- [51] E. Gaggelli, F. Berti, N. D'Amelio, N. Gaggelli, G. Valensin, L. Bovalini, A. Paffetti, L. Trabalzini, *Environ. Health Perspect.* **2002**, *110*, 733–738.
- [52] S. J. Dougan, A. Habtemariam, S. E. McHale, S. Parsons, P. J. Sadler, *Proc. Natl. Acad. Sci. USA* **2008**, *105*, 11628–11633.
- [53] M. S. Costa, Y. G. Gonçalves, S. C. Teixeira, D. C. de O. Nunes, D. S. Lopes, C. V. da Silva, M. S. da Silva, B. C. Borges, M. J. B. Silva, R. S. Rodrigues, V. de M. Rodrigues, G. Von Poelhsitz, K. A. G. Yoneyama, *J. Inorg. Biochem.* **2019**, *195*, 1–12.
- [54] G. Jiang, W. Zhang, M. He, Y. Gu, L. Bai, Y. Wang, Q. Yi, F. Du, *Spectrochim. Acta A Mol.* **2019**, *220*, 117132.
- [55] A. Aranda, L. Sequedo, L. Tolosa, G. Quintas, E. Burello, J. V. Castell, L. Gombau, *Toxicol. in Vitro* **2013**, *27*, 954–963.
- [56] W. Li, G.-B. Jiang, J.-H. Yao, X.-Z. Wang, J. Wang, B.-J. Han, Y.-Y. Xie, G.-J. Lin, H.-L. Huang, Y.-J. Liu, *J. Photochem. Photobiol. B* **2014**, *140*, 94–104.
- [57] S. Karmakar, K. Purkait, S. Chatterjee, A. Mukherjee, *Dalton Trans.* **2016**, *45*, 3599–3615.
- [58] B. I. Tarnowski, F. G. Spinale, J. H. Nicholson, *Biotech. Histochem* **1991**, *66*, 296–302.
- [59] M. K. Mohamed Subarkhan, L. Ren, B. Xie, C. Chen, Y. Wang, H. Wang, *Eur. J. Med. Chem.* **2019**, *179*, 246–256.
- [60] H. Bregman, P. J. Carroll, E. Meggers, *J. Am. Chem. Soc.* **2006**, *128*, 877–884.
- [61] W. Guo, W. Zheng, Q. Luo, X. Li, Y. Zhao, S. Xiong, F. Wang, *Inorg. Chem.* **2013**, *52*, 5328–5338.
- [62] J. É. Debreczeni, A. N. Bullock, G. E. Atilla, D. S. Williams, H. Bregman, S. Knapp, E. Meggers, *Angew. Chem. Int. Ed.* **2006**, *45*, 1580–1585; *Angew. Chem.* **2006**, *118*, 1610–1615.
- [63] S. Bhattacharyya, K. Purkait, A. Mukherjee, *Dalton Trans.* **2017**, *46*, 8539–8554.
- [64] APEX3 “Program for Data Collection on Area Detectors” BRUKER AXS Inc., 5465 East Cheryl Parkway, Madison, WI 53711-5373 USA.
- [65] G. M. Sheldrick, *Acta Crystallogr. Sect. A* **2008**, *64*, 112–122.
- [66] G. M. Sheldrick, *Acta Crystallogr. Sect. A* **2015**, *71*, 3–8.
- [67] G. M. Sheldrick, *Acta Crystallogr. Sect. C* **2015**, *71*, 3–8.
- [68] O. V. Dolomanov, L. J. Bourhis, R. J. Gildea, J. A. K. Howard, H. Puschmann, *J. Appl. Crystallogr.* **2009**, *42*, 339–341.

Manuscript received: November 14, 2020

Revised manuscript received: December 21, 2020

Accepted manuscript online: January 6, 2021

Version of record online: March 12, 2021